OULU 2015
C 534

ACTA UNIVERSITATIS OULUENSIS

Jhih-Fong Lin

MULTI-DIMENSIONAL CARBONACEOUS COMPOSITES FOR ELECTRODE APPLICATIONS

UNIVERSITY OF OULU GRADUATE SCHOOL;
UNIVERSITY OF OULU,
FACULTY OF INFORMATION TECHNOLOGY AND ELECTRICAL ENGINEERING,
DEPARTMENT OF ELECTRICAL ENGINEERING

ACTA UNIVERSITATIS OULUENSIS
C Technica 534

JHIH-FONG LIN

MULTI-DIMENSIONAL CARBONACEOUS COMPOSITES FOR ELECTRODE APPLICATIONS

Academic dissertation to be presented with the assent of the Doctoral Training Committee of Technology and Natural Sciences of the University of Oulu for public defence in the OP auditorium (L10), Linnanmaa, on 25 June 2015, at 12 noon

UNIVERSITY OF OULU, OULU 2015

Acta Univ. Oul. C 534, 2015

Supervised by
Professor Krisztian Kordas
Professor Wei-Fang Su

Reviewed by
Professor Thomas Wågberg
Doctor Tanja Kallio

ISBN 978-952-62-0844-2 (Paperback)
ISBN 978-952-62-0845-9 (PDF)

ISSN 0355-3213 (Printed)
ISSN 1796-2226 (Online)

Cover Design
Raimo Ahonen

JUVENES PRINT
TAMPERE 2015

Lin, Jhih-Fong, Multi-dimensional carbonaceous composites for electrode applications.
University of Oulu Graduate School; University of Oulu, Faculty of Information Technology and Electrical Engineering, Department of Electrical Engineering
Acta Univ. Oul. C 534, 2015
University of Oulu, P.O. Box 8000, FI-90014 University of Oulu, Finland

Abstract

The objective of this thesis is to demonstrate multi-dimensional carbon nanotube (CNT) structures in combination with various active materials in order to evaluate their performance in electrode applications such as cold emitters, electric double-layer capacitors (EDLC), and electrochemical sensor/catalyst devices.

As the host materials for other active materials, the construction of multi-dimensional CNT nanostructures in this thesis is achieved by two different approaches. In the first, direct growth of 3-dimensional carbon nanostructures by catalytic chemical deposition to produce filamentary carbon as well as vertically aligned forests was applied. The second route that was utilized encompassed the immobilization of CNTs from dispersions to form 2-dimensional surface coatings as well as self-supporting porous buckypapers. Carbonaceous nanocomposites of the active materials are obtained by a number of different methods such as (i) growing nanotubes and filamentous structures on porous Ni catalyst structures, (ii) impregnating CNTs with organic receptor molecules or with Pd nanoparticles, (iii) plating and replacing Cu with Pd on the nanotubes by chemical and galvanic reactions, (iv) annealing W evaporated on CNTs to form CNT-WC composites in solid-solid reactions and (v) reacting S vapor with W coated on CNTs to synthesize CNT-WS_2 edge-on lamellar structures of the dichalcogenide in the vertically aligned CNT forests.

The 3-dimensional carbon-Raney®Ni composite electrodes show reasonable specific capacitance of ~12 $F \cdot g^{-1}$ in electric double-layer capacitors as well as a low turn-on field (<1.0 $V \cdot \mu m^{-1}$) in field emitter devices. CNT-Nafion®-trifluoroacetylazobenzene coatings on glassy carbon electrodes outperform their Nafion®-trifluoroacetylazobenzene counterparts in electrochemical sensing of different amine compounds (e.g. 10 mM cadaverine, putrescine or ammonia). Cu and CuPd/buckypaper composites display catalytic activity in electrocatalytic oxidation of methanol in alkaline media. On the other hand, nanocomposites of WC and WS_2 with aligned CNT forest exhibit a promising performance in hydrogen evolution reactions with an overpotential between -0.5 and -0.7 V at pH~1. In addition, these respective CNT forest aligned nanocomposites also demonstrate a novel method to obtain macroscopic 3-dimensional catalytic electrode assemblies.

The results in this thesis elucidate the combination of carbon based nanostructures with organic and inorganic materials as a feasible and versatile approach to produce electrodes for several applications. The following studies of each active carbonaceous composite are expected to boost the technological innovation in relevant fields and initiate further development for commercial exploitation.

Keywords: carbon nanotube, catalyst, cold emitter, electric double-layer capacitor, electrocatalytic hydrogen production, electrochemical sensor, methanol oxidation, nanocomposites

Lin, Jhih-Fong, Moniulotteiset hiiltä sisältävät komposiitit elektrodisovelluksiin.
Oulun yliopiston tutkijakoulu; Oulun yliopisto, Tieto- ja sähkötekniikan tiedekunta, Sähkötekniikan osasto
Acta Univ. Oul. C 534, 2015
Oulun yliopisto, PL 8000, 90014 Oulun yliopisto

Tiivistelmä

Työn tavoitteena oli demonstroida moniulotteisia hiilinanoputkirakenteita (CNT), joihin yhdistetään erilaisia aktiivisia materiaaleja sekä arvioida niiden suorituskykyä elektrodisovelluksissa, kuten kenttäemitterissä, sähköisissä kaksoiskerroskondensaattoreissa ja sähkökemiallisissa anturi- ja katalyyttikomponenteissa.

Moniulotteisten CNT-nanorakenteiden konstruoiminen muiden aktiivisten materiaalien isäntämateriaaliksi toteutettiin kahdella tavalla. Ensimmäisessä toteutuksessa sovellettiin katalyyttiskemiallista pinnoitusta, jolla kasvatettiin suoraan kolmiulotteisia hiilinanorakenteita sekä kuitumaisena hiilenä että pystysuuntaan orientoituneina hiilinanoputkimetsinä. Toinen päämenetelmä oli hiilinanoputkien immobilisointi dispersioista kaksiulotteisiksi pinnoitteiksi ja itsetukeutuviksi huokoisiksi hiilinanoputkipapereiksi. Hiiltä sisältäviä aktiivisten materiaalien nanokomposiitteja valmistettiin useilla menetelmillä, kuten (i) kasvattamalla nanoputkia ja kuitumaisia rakenteita huokoisiin Ni-katalyyttirakenteisiin, (ii) kyllästämällä hiilinanoputkia orgaanisilla reseptorimolekyyleillä tai Pd-nanopartikkeleilla, (iii) pinnoittamalla ja korvaamalla nanoputkien päällä olevaa kuparia palladiumilla kemiallisten ja galvaanisten reaktioiden avulla, (iv) hehkuttamalla hiilinanoputkien pinnalle höyrystettyä wolframia (W) muodostamaan CNT-WC-komposiitteja kiinteä–kiinteä-reaktiolla sekä (v) antamalla rikkihöyryn reagoida W-pinnoitettujen hiilinanoputkien kanssa lamellaaristen CNT-WS_2-kalkogenidirakenteiden syntetisoimiseksi pystysuuntaan orientoituneisiin CNT-metsiin.

Kolmiulotteisilla hiili–Raney®Ni-komposiittielektrodeilla saavutetaan kohtuullinen ominaiskapasitanssi (~12 $F \cdot g^{-1}$) sähköisissä kaksoiskerroskondensaattoreissa ja pieni kytkeytymiskenttä (<1,0 $V \cdot \mu m^{-1}$) kenttäemitterikomponenteissa. CNT-Nafion®-trifluoroasetyyliatsobentseeni-pinnoitteet lasimaisilla hiilielektrodeilla ovat selvästi parempia erilaisten amiiniyhdisteiden (esimerkiksi 10 mM kadaveriini, putreskiini tai ammoniakki) sähkökemiallisessa havaitsemisessa kuin vastaavat Nafion®-trifluoroasetyyliatsobentseeni-pinnoitteet. Cu- ja CuPd-hiilinanoputkipaperikomposiitit osoittavat katalyyttistä aktiivisuutta metanolin sähkökatalyyttisessä hapettumisessa emäksisessä väliaineessa. Toisaalta WC- ja WS_2-yhdisteiden ja orientoituneiden CNT-metsien muodostamat nanokomposiitit osoittavat lupaavaa suorituskykyä vedynmuodostamisreaktiossa -0,5…-0,7 V ylipotentiaalilla, ja nämä myös demonstroivat uutta menetelmää makroskooppisten kolmiulotteisten katalyyttisten elektrodirakenteiden toteuttamiseksi.

Väitöskirjan tulokset osoittavat, että hiilipohjaisten nanorakenteiden ja orgaanisten/epäorgaanisten materiaalien yhdistäminen on toteuttamiskelpoinen ja monipuolinen lähestymistapa elektrodien valmistamiseksi useisiin sovelluksiin. Kunkin työssä esitetyn aktiivista hiiltä sisältävän komposiitin tutkimuksen odotetaan lisäävän kyseisen alan teknisiä innovaatioita ja synnyttävän lisää kehitystyötä tutkimuksen kaupalliseksi soveltamiseksi.

Asiasanat: hiilinanoputki, katalyytti, kylmäemitteri, metanolin hapetus, nanokomposiitit, sähköinen kaksoiskerroskondensaattori, sähkökatalyyttinen vedyn tuotanto, sähkökemiallinen anturi

“Luck is what happens when preparation meets opportunity.” Lucius Annaeus Seneca

Acknowledgements

First of all, I would like to express my appreciation to my supervisor, Prof. Krisztian Kordas for the help and support throughout this thesis work. Without your guidance, the work in its entirety would not have been carried out in such short time. I thank you for your invaluable suggestions that allowed me to become a better independent researcher with required skills, a team player who can work with others effectively and a brave man who can now face the unknown future with self–confidence.

Secondly, I would like to express my sincere thanks to another co–supervisor Prof. Wei–Fang Su as well as to Dr. Ming–Chung Wu, Dr. Geza Toth, Dr. Melinda Mohl, Doc. Antti Uusimäki, Aron Dombovari, Olli Pitkänen, Anne–Riikka Rautio, Robert Puskas and colleagues in the Laboratory helping my work. I would like to express my gratitude to Prof. Heli Jantunen for your contribution to bringing about the dual–degree program. This program provided me with the chance to conduct another independent postgraduate research project with a different thesis topic here. The experiences gained through these years will be the most valuable treasure in my life.

Additionally, the valuable discussion and technical support from Prof. Akos Kukovecz and Prof. Zoltan Konya at University of Szeged, Dr. Robert Vajtai and Prof. Pulickel Ajayan at Rice University, Prof. Tomi Laurila at Aalto University and Prof. Jyri–Pekka Mikkola at Umeå University are highly appreciated as well. The importance of your help should also be comprehensively addressed for this thesis work.

This work was carried out at the Microelectronics and Materials Physics Laboratories between 2012 and 2015. The work was financially supported by the Academy of Finland, Tekes and EU FP7 program.

Last, but most certainly not least, I would like to express my thanks to my family members especially my parents who supported and encouraged me during this long period of study. Finally, the deepest gratitude is forwarded to Hui–Ya for your patience when I was busy with my own work and the accompaniment that you provided during difficult times.

Thank you all!

Oulu, May 2015 Jhih–Fong Lin

Original publications

This thesis is based on the following publications, which are referred throughout the text by their Roman numerals:

I Lin JF, Mohl M, Nelo M, Toth G, Kukovecz Á, Kónya Z, Sridhar S, Vajtai R, Ajayan PM, Su WF, Jantunen H & Kordas K (2015) Facile synthesis of nanostructured carbon materials over Raney® nickel catalyst films printed on Al_2O_3 and SiO_2 substrates. Journal of Materials Chemistry C 3(8): 1823–1829.

II Lin JF, Kukkola J, Sipola T, Raut D, Samikannu A, Mikkola, JP, Mohl M, Toth G, Su WF, Laurila T & Kordas K (2015) Trifluoroacetylazobenzene for optical and electrochemical detection of amines. Journal of Materials Chemistry A 3(8): 4687–4694.

III Lin JF, Mohl M, Toth G, Puskás R, Kukovecz Á & Kordas K (2015) Electrocatalytic properties of carbon nanotubes decorated with copper and bimetallic CuPd nanoparticles. Topics in Catalysis. Manuscript.

IV Lin JF, Pitkänen O, Mäklin J, Puskas R, Kukovecz A, Dombovari A, Toth G & Kordas K (2015) Synthesis of tungsten carbide and tungsten disulfide on vertically aligned multi–walled carbon nanotube forests and its application as non–Pt electrocatalyst for the hydrogen evolution reaction. Journal of Materials Chemistry A. In press.

The majority of the experiments described in the dissertation were planned by Lin JF, Mohl M, Toth G and Kordas K. Synthesis of the materials (except CNT growth) and their characterization (X–ray diffraction, scanning and transmission electron microscopy, Raman and UV–Vis spectroscopy and cyclic voltammetry) were carried out by Lin JF. The growth of CNT and other carbonaceous materials were made possible with the contributions of Pitkänen O and Mäklin J. High–resolution transmission electron microscopy and thermogravimetric analysis were performed by Puskás R (University of Szeged). The field emission measurements were conducted by Sridhar S (Rice University). The results were discussed and evaluated together with the co–authors. Each original paper has been written by Lin JF with the help of the co–authors.

Contents

1 Objective and outline of thesis

The main objectives of this thesis are to establish various kinds of synthetic approaches of nanostructured carbon based composites and then to demonstrate applications, where the nanocomposites are used as electrode materials.

The first section of this thesis introduces various forms of sp^2 hybridized carbon nanomaterials followed by a more detailed overview of carbon nanotubes (CNTs) with a focus on their electrical and mechanical properties. The final part of this chapter also summarizes the growth of filamentary carbon nanomaterials and their use in the construction of multidimensional nanostructures.

In Chapter 2, the synthetic process of three–dimensional carbonaceous electrodes by combining catalyst printing and subsequent chemical vapor deposition (CVD) of carbon is described. Mesoporous Ni films made of Raney® nickel catalyst based pastes are applied as growth templates for nanostructured carbon materials grown at different temperatures from an acetylene precursor. The obtained 3–dimensional Ni–carbon composites are studied as electrodes for EDLCs and cold emitters (Paper I).

Chapter 3, based on Paper II, discusses the use of trifluoroacetylazobenzene (known as an amine receptor) as an optical and electrochemical sensing material to detect various types of amine compounds. In the electrochemical measurements, 2–dimensional composite coatings of the organic amine receptor with Nafion® and Nafion®–CNT are studied and compared to reveal their sensitivity upon exposure to a number of different amines in aqueous electrolytes.

In Chapter 4, Cu and CuPd catalysts are grown on Pd decorated CNT films (buckypapers) by chemical plating and subsequent galvanic replacement. Both Cu and CuPd/buckypaper composites are evaluated as electrode materials in the electrocatalytic oxidation of methanol. The possible oxidation mechanisms and durability of the composites are also presented (Paper III).

Chapter 5 describes a novel template route to grow tungsten carbide (WC) and tungsten disulfide (WS_2) nanoparticles on vertical aligned CNTs. The work discusses on the formation, structure and electrocatalytic behavior of the CNT–WC and CNT–WS_2 composites in hydrogen evolution reactions (Paper IV).

In Chapter 6, the major findings of the thesis are summarized, and an outlook for relevant further studies is herein provided.

2 Introduction of carbonaceous nanomaterials

Carbon, a tetravalent, nonmetallic element, exists in several famous allotropes such as diamond, graphite, fullerenes, carbon nanotubes and graphene. These allotropes vary due to their different atomic bonding and crystal symmetry. The very different nature (physical and chemical properties) of these carbon allotropes clearly demonstrates how atomic arrangement may affect the properties of materials. Discoveries of sp^2 hybridized carbon nano–allotropes such as fullerene, (Kroto *et al.* 1985) carbon nanotubes, (Iijima 1991) and graphene (Novoselov *et al.* 2004) over the past few decades has triggered considerable research in materials science leading to a great development in photonics, electronics and photovoltaics. The sp^2 atomic bonding structure results in excellent in–plane transport of carriers. Even ballistic transport over a micrometer in length has been demonstrated in CNTs, which is extraordinary considering the rise of scattering in metals after a few nanometers. Combining this feature with the high optical transmittance of easily percolating thin networks of carbon nanotubes and graphene, transparent electrodes were demonstrated to replace costly indium tin oxide. (Zhang *et al.* 2005, Wang *et al.* 2008, Kim *et al.* 2009, Bae *et al.* 2010) On the other hand, these carbon allotropes have also been proposed for nanoelectronic applications as high–speed field–effect transistors, owing to the large carrier mobility (μ) in these materials. For example, fullerene thin films grown epitaxially (Anthopoulos *et al.* 2006) (μ=6 $cm^2V^{-1}S^{-1}$) or via solution–processing alignment (Li *et al.* 2012) (μ=11 $cm^2V^{-1}S^{-1}$) have been proven to be competitive n–channel field–effect transistors amongst various organic materials. Considering their colossal carrier mobility, carbon nanotubes (Durkop *et al.* 2004) and graphene (Morozov *et al.* 2008, Bolotin *et al.* 2008) (μ=7.9×10^4 and 2.0×10^5 $cm^2V^{-1}S^{-1}$, respectively) were expected to replace silicon (Takagi *et al.* 1994) (μ<1000 $cm^2V^{-1}S^{-1}$) in p–channel and bipolar field–effect transistors of logic architectures. By combining the superior electrical properties with their tiny size, (~1 nm in diameter for fullerenes and single–wall CNTs, and only one carbon atom thick structures for graphene), and outweighed specific surface area (~2800 $m^2{\cdot}g^{-1}$ for C60 fullerene (Adams *et al.* 1994), ~2.200 $m^2{\cdot}g^{-1}$ for opened single–walled carbon nanotubes (Hiraoka *et al.* 2010) and 2630 $m^2{\cdot}g^{-1}$ for graphene (Stoller *et al.* 2008)), the application of these materials is extremely beneficial in various interfacial reactions with charge exchange. For example, the derivatives of fullerenes such as [6,6]–phenyl–C61–butyric acid methyl ester ($PC_{61}BM$), [6,6]–phenyl–C71–butyric acid methyl ester and ($PC_{71}BM$) have been exploited as electron acceptors in organic bulk–heterojunction

photovoltaics with very competitive power conversion efficiencies (~10%). (Lai *et al.* 2014) However, carbon nanotubes, graphene and their functionalized derivatives were also eminent candidates for electrodes in electrochemical (Stoller et al. 2008, Wang 2005, Lee *et al.* 2009, Gong *et al.* 2009, Hou *et al.* 2010, Shao *et al.* 2010, El–Kady *et al.* 2012, Wang *et al.* 2010) and p–type co–catalysts in photocatalytic (Woan *et al.* 2009, Zhang *et al.* 2011) applications due to their huge contact surface area with reactants, which could noticeably enhance the corresponding reaction yield. In addition, carbon nanotubes and graphene are also employed to construct conductive three–dimensional structures such as graphene sponges, (Vickery *et al.* 2009, Chen *et al.* 2011, Nguyen *et al.* 2012, Hu *et al.* 2013) aligned CNT forests, (Wei *et al.* 2002, Correa–Duarte *et al.*2004) random networks, (Fu *et al.* 2012) and carbon nanotube/graphene sandwich structures. (Fan *et al.* 2010) These three–dimensional carbonaceous structures not only inherit the superior properties of their components, (carbon nanotube and/or graphene) which are listed above but also possess excellent mechanical strength and elasticity (Vickery *et al.* 2009, Chen *et al.* 2011, Hu *et al.* 2013) as well as controllable porosity. (Nguyen *et al.* 2012)

2.1 Introduction to CNTs

Carbon nanotubes are composed of hexagonally arranged covalently bonded sp^2 carbon atoms that are located on a surface of a cylinder (schematically, if a graphene sheet would be rolled–up into a cylindrical structure). Carbon nanotubes can be simply categorized as single–wall carbon nanotubes (SWCNTs), double–walled carbon nanotube (DWCNTs) and multi–walled carbon nanotube (MWCNTs) depending on the number of graphene layers wrapped around on each other. The cylindrical structure, diameter, helicity of graphene layers in the wall, number of graphene layers in walls, and possible defects have significant implications on the electrical as well as mechanical properties of these nanostructures.

When folding the hexagonal lattice to form a cylinder (while matching sites on the edges), we can obtain SWCNTs of different kinds due to the helicity of carbon atoms in the nanotube and of course to the diameter of the structure. Mathematically, this can be presented by a chiral vector (a vector between two crystallographically equivalent carbon atoms being folded in each other) as $\boldsymbol{C} = n\boldsymbol{a} + m\boldsymbol{b}$, where $\boldsymbol{a}$ and $\boldsymbol{b}$ are the unit vectors in a hexagonal lattice; n and m are integers. For m = 0, the SWCNT is called “zigzag” CNT; for n = m, it is “armchair”; in all other instances it is called “chiral”. The parameters n and m determine not only the chirality but

also the diameter of the nanotubes. Furthermore, calculations derived from the two–dimensional energy dispersion relation for periodic carbon π orbitals indicated that the wrapping direction and diameter of single–walled carbon nanotube would greatly influence its electronic structure. (Saito *et al.* 1992) Accordingly, if 2n + m = 3q (where q is an integer) the nanotube is metallic, otherwise semiconducting (band gaps can vary from a few tens of meV up to ~1 eV in practice).

Double–walled carbon nanotubes, which are consisted of two coaxial tubes, possess similar chirality–dependent carrier transport. (Liu *et al.* 2009, Fujisawa *et al.* 2011) The outer tube could significantly improve its chemical resistivity by protecting the inner tube away from the induced defects during the functionalization (grafting of functional group would break the C=C bond) in corresponding applications without sacrificing its conductivity. On the other hand, because the band gap of a semiconducting nanotube is inversely proportional to its diameter, (Ajiki *et al.* 1993) the increasing number of wrapping graphene layers (interlayer distance ~3.4 Å) result in a significant decrease in the band gap. Furthermore, as conduction occurs mainly in the outermost graphene layer (viz. the inner layers are separated by tunneling barriers) (Bourlon *et al.* 2004) multi–walled carbon nanotubes show semi–metallic or metallic behavior.

In practical applications, the use of SWCNTs in p–type field–effect transistors (Durkop *et al.* 2004) or other logic devices such as NEMs (Sazonova *et al.* 2004, Loh *et al.* 2012, Shulaker *et al.* 2013) could substantially increase the speed of devices due to its small size and giant mobility. Efforts to find CNTs as successors of silicon chips, which will soon encounter physical limits of improving further, are still limited to laboratory experiments, since several important issues should be addressed before the commercialization: (i) controllable synthesis process to produce tubes with the same diameter and chirality (n,m) hence controlled electrical properties; (ii) development of large scale synthesis with well–defined surface locations of the CNTs on substrates to allow scalable integration of devices, and (iii) improvement of nanotube quality control, manipulation and electrical/mechanical interfacing. (Arnold *et al.* 2006, Liu *et al.* 2010, Zhang *et al.* 2011, Chen *et al.* 2014)

Carbon nanotubes as 1–dimensional objects with high aspect ratios and good electrical conductivity (Ebbesen *et al.* 1996) could effectively lower the percolation thresholds for carrier transport in films and fibers as compared to 0–dimesnional nanoparticle networks. In recent years, the successful synthesis (Vigolo *et al.* 2000, Dalton *et al.* 2003, Ericson *et al.* 2004) of spun carbon fiber not only retains the excellent properties (6.7×10^8 $S\cdot cm^{-1}$ in conductivity (Zhao *et al.* 2011)) of CNTs

but also opens up new horizons in various macroscopic applications such as conducting cables, (Zhao *et al.* 2011) actuators, (Foroughi *et al.* 2011, Guo *et al.* 2013) flexible photovoltaics (Chen *et al.* 2011) and fiber–based wearable electronics (Zeng *et al.* 2014).

The mechanical properties of carbon nanotubes have been measured by a number of different parameters including thermally (Treacy *et al.* 1996) and field induced (Poncharal *et al.* 1999) vibration of MWCNTs as cantilevers, transversal mechanical loading with an atomic force microscope tip while simultaneously measuring deformation and force (Wong *et al.* 1997, Salvetat *et al.* 1999), as well as by direct tensile loading (Yu *et al.* 2000). The values of the Young's modulus and strength are elucidated to be 0.18–1.28 TPa and 1.4–14 GPa, respectively. The responses of multi–walled carbon nanotubes to form high–strain deformations, like reversible bending as well as buckling without further severe damages, also suggest that nanotubes are extraordinarily flexible and resilient (Wong *et al.* 1997, Falvo *et al.* 1997). In the case of SWCNTs, ropes rather than individual nanotubes were studied due to the difficulty of manipulation, (Salvetat *et al.* 1999, Yu *et al.* 2000) and the Young's modulus was evaluated to be ~1 TPa which is similar to that of graphite in–plane (1 TPa) (Kelly *et al.* 1981). Furthermore, the tensile strength and strain of these ropes can reach as high as 52 GPa (mean value 30 GPa) and 5.3%, respectively. (Yu *et al.* 2000) Even though the outstanding mechanical properties of carbon nanotubes (demonstrated above) are highly expected to replace the commercial construction materials like steel, there is still a long way to go for large scale production of carbon nanotube products with macroscopic dimensions. On the other hand, the tiny dimensions of carbon nanotubes make them suitable as reinforcing elements to enhance the mechanical strength of various composites due to their high surface area, which would greatly enhance the interaction with composite matricies. (Coleman *et al.* 2006, Rogers *et al.* 2010, Naraghi *et al.* 2010, Naraghi *et al.* 2013, Espinosa *et al.* 2013) However, in various carbon–based composites with a high density of nanotube loading, the weak shear interaction between adjacent SWCNTs in ropes or adjacent graphitic layers in MWCNTs (van der walls force, 2.3×10^{-14} N per atom (Cumings *et al.* 2000)) is often a problem. One potential way of overcoming the easy sliding of the carbon layers may be obtained by inter–tube linking or by establishing crosslinking bonds between adjacent sheets for instance by radiation damage of the structures. (Kis *et al.* 2004, Peng *et al.* 2008)

2.2 Synthesis, organization and immobilization of filamentary carbon nanomaterials

In general, filamentary carbon nanomaterials are categorized as carbon nanofiber or carbon nanotube depending whether the structure is hollow or not. Although both carbon nanofibers and nanotubes have similar cylindrical structures, carbon nanofibers are considered to have a lower degree of graphitic bonding due to the lower growth temperature. With the development of petrochemistry in the last century, carbon nanofibers were first taken as by–products of the deactivation of catalysts in hydrogenation/dehydrogenation of hydrocarbons. R. T. K. Baker and co–workers found various types of filamentary or angular graphite laminae on nickel catalysts after the decomposition of acetylene. (Baker *et al.* 1972) Similar works on the catalytic decomposition of hydrocarbons over different transition metal catalysts were studied with the main focus of catalyst poisoning (coking) at that time. (Pinilla *et al.* 2011, Pinilla *et al.* 2011) Tailoring the properties and structures of carbon nanofibers could be achieved by careful control of several parameters (Rodriguez *et al.* 1995) to produce industrial scale quantities of high–quality carbon nanofibers (De Jong *et al.* 2000, Pham–Huu *et al.* 2002)

Carbon nanotubes are obtained in a similar way as nanofibers (i.e. with a decomposition of a carbon source in the presence of a catalyst). However, the major difference in this respective production is the smaller size of the catalyst and higher temperature for synthesis. The three principal methods for carbon nanotube synthesis are (i) arc discharge, (ii) laser ablation and (iii) chemical vapor deposition. CNTs synthesized by arc discharge and laser ablation are mainly in the form of powder. On the other hand, with the application of catalyst templates, chemical vapor deposition can provide a facile approach to obtain ordered structures such as vertical–aligned forests (Hata *et al.* 2004), horizontally aligned arrays (Zhang *et al.* 2001, Ibrahim *et al.* 2012) and complex three–dimensional (3D) microarchitectures. (Halonen *et al.* 2010) Chemical vapor deposition is a collective name for the growth procedure based on catalytic decomposition of carbonaceous vapors or gases at high temperatures (usually between 600–1200°C). Plasma–assisted processes can enhance the dissociation of carbonaceous precursors and lower growth temperatures. (Chowalla *et al.* 2001)

Immobilization of carbon nanomaterials on surfaces is a multi–step process which includes (i) dispersion of carbon nanomaterials in solvents after functionalization and/or addition of surfactants to eliminate the surface tension between immiscible bulk phases (O'Connell *et al.* 2001, Zhenng *et al.* 2003, Li *et*

al. 2008) and (ii) casting of functionalized carbon nanomaterials, which entails the deposition (e.g. by filtration and spin coating), using various printing techniques (e.g. stencil, screen, inkjet) or spray coating on a desired substrate. The major advantages of the aformentioned solution–accessible techniques are scalability, direct production of micropatterned structures and wide range of options for substrate selection. Various carbonaceous thin films have been made by this approach and applied as electrodes, (Li *et al.* 2003, Eda *et al.* 2008) sensors, (Kordas *et al.* 2006) interconnects and transistors. (Mustonen *et al.* 2008, Gracia *et al.* 2010) However, incorporated functional groups and surfactants are hard to be detached from the immobilized carbon nanostructures and may deteriorate the properties of carbon nanomaterials, resulting in a drawback in some applications. (Awasthi *et al.* 2009, Gulotty *et al.* 2013)

Carbonaceous nanostructures can be also obtained through the introduction of carbon nanomaterials to templates. (Cao *et al.* 2011, Wu *et al.*2013) Generally, two different kinds of templates, i.e. hard and soft are utilized as molds to create the porous carbonaceous structure. In the hard template method, inorganic oxides such as zeolites (Férey *et al.*1999, Yang *et al.* 2007), clays (Kyotani *et al.* 1994) anodic aluminum oxides (Meng *et al.* 2005) and silica (Lee *et al.* 1999, Han *et al.* 2000) offer a removable rigid frame to replicate carbonaceous materials with controllable porosity (the carbon source is simply decomposed in the template at high temperature). On the other hand, impregnation of catalysts (e.g. Fe, Co, Ni and their combinations) into the template or using template materials with catalytic activity for carbon growth are also a feasible approach to build up a porous carbonaceous structure. Although such three–dimensional carbonaceous networks synthesized by catalytic growth do not necessarily copy the original structure of the template, the typically high graphitic structure and good mechanical integrity of the obtained composites still offer a number of different practical benefits for applications.

In soft templates, the self–assembly of structure–directing agents (i.e. surfactants or copolymers) and carbon precursors in hybrid solutions provide another approach to the acquisition of flexible, porous carbonaceous structures. However, the porosity of carbon structures derived from the soft template method highly depends on the temperature, solvent and ionic interaction and only a few successful studies have been reported. (Liang *et al.* 2004, Liang *et al.* 2006*)* The products synthesized from traditional template carburization have advantages such as large specific surface area, well–controlled porosity and pore size which allow their utilization in sensors, (Lai *et al.* 2007) electrodes for energy storage, (Lee *et al.* 1999, Joo *et al.* 2001, Zhou *et al.* 2003) hydrogen storage material (Yang *et al.*

2007) and sorbent materials for contaminants and drugs. (Hartmann *et al.* 2005, Gu *et al.* 2007)

2.3 Synthesis of active carbonaceous composites by integrating different nanomaterials upon filamentary carbon host

As described above, carbon nanomaterials possess large surface area, superior electrical and mechanical properties as well as great chemical inertness suitable for various applications. Depending on the particular application however, often other functional materials are incorporated in the carbon host in order to improve a specific physicochemical property (e.g. catalytic activity, electrical conductivity, work function, morphology, mechanical hardness) of the original material. In this thesis, various types of active materials are immobilized on the synthesized carbon host to form nanocomposites e.g. by impregnating CNTs with polymers or with metal nanoparticles, (ii) chemically plating metals and galvanically replacing those with other metals of higher standard redox potential and (iii) annealing metal coated CNTs in inert and reactive atmospheres.

First of all, direct mixing of active materials with carbon host are common techniques to introduce organic molecules (Moniruzzaman *et al.* 2006) and inorganic nanoparticles. (Yao *et al.* 2008) The solubility of carbon host (Chen *et al.* 2008 and 2002) and nanoparticles (Lin *et al.* 2013) in solution phase is critical to ensure the formation of homogeneous mixtures by preventing severe phase separation. Accordingly, surface engineering to tune surface energy and wetting behaviour is an important part of most of the synthetic processes. Using stable dispersions/solutions of the carbon host and active materials has a further practical advantage in reference to dry processes. Namely, it is the enabled large–scale production of composite coatings and films by a variety of printing, casting, spraying and painting methods.

Secondly, the impregnation of metal nanoparticles upon carbon host with subsequent crystal growth is another feasible approach to acquire active carbonaceous composites. The impregnation of metal nanoparticles on carbon host is usually conducted by several steps: functionalization of carbon materials, mixing functionalized carbon host with metal–organic complex in organic solvent, calcination and reduction.(Leino *et al.* 2013) The impregnated nanoparticles can be directly taken as catalyst for carbon growth,(Fan *et al.* 2010) electrocatalytic material for decomposition of small organic molecules(Hu *et al.* 2012) as well as receptor for electrochemical sensing.(Guo *et al.* 2010)

The amount and cost of the anchored metals on carbons are also important issues in practice. Today's trends in developing noble–metal free catalyst composites have triggered the use of chemical plating for depositing for instance Cu (Xu *et al.* 2004) and Ni (Li *et al.* 1997) nanoparticles on CNTs. The chemical plating process provides a simple approach to obtain metal nanostructures on the carbon host from solutions of complexed metal ions and reducing agents. Furthermore, galvanic replacement reactions can be applied in a subsequent process to partially remove the original metal and simultaneously introduce another metal thus creating bimetallic catalyst structures. Such a galvanic replacement reaction takes place, when the redox potential of the replacing metal is higher than that of the original one.

Last, the growth of metal carbides and sulphides from pure metals in reactive atmospheres (Davidson *et al.* 1978; Li *et al.* 2003) or from suitable precursors in solvothermal conditions (Ratha *et al.* 2013, Singla *et al.* 2015) offer further alternatives to produce noble–metal free catalysts. The application of any of the above methods in the presence of a carbon support can lead to composites of the carbon host and the metal compounds as it is demonstrated in this thesis.

3 Growth of three–dimensional carbonaceous electrodes and its application in electrochemical storage and field emission

In this chapter, background information on the utilization of CNTs in electrochemical storage and field emission is provided, and the synthesis along with the characterization and utility of three–dimensional carbonaceous mesoporous nanostructures is described. The results were originally presented in Paper I.

3.1 Background

In the past decade, the fast–growing market of mobile devices and electrically powered vehicles urged needs for high–power energy storage devices. Supercapacitors with high power capability and relatively large energy density (Simon *et al.* 2008) offer a promising approach to meet these demands. According to the energy storage mechanism, supercapacitors can be divided into two categories. One is the electrical double–layer capacitor (EDLC) in which the charges are electrostatically accumulated at the interface between electrolyte and electrode. As a result, the efficiency of device is highly dependent on accessible surface area to electrolyte ions and also on the electrical conductivity of the electrode material. (Halonen *et al.* 2013, Rauto *et al.* 2015) The other class is that of pseudocapacitors (not covered in this work), where the electrical energy is stored by fast and reversible faradic processes between redox–active species (e.g. ruthenium oxides) and an electrolyte.

The concept of the EDLC was first modeled by Hermann von Helmholtz (Helmholtz *et al.* 1853) in 1853 and explicitly confirmed by Stern (Stern *et al.* 1924) in 1924 with modification. In Stern's modified model, the distribution electrolyte ion around the electrode can be recognized by two distinctive regions: a compact layer and a diffuse layer. For the compact layer, there is a correspondence to the distance of a depletion region where only oppositely charged ions are adsorbed on the electrode. As a result, the capacitance of EDLC can be treated as a combination of the capacitances from two regions in series (C_H and C_{diff} for compact and diffuse layers, respectively). Although the concept of infinite parallel electrodes is often used to estimate the capacitance, such a simple linear relationship cannot hold for highly porous electrodes since the limited space in the porous structure would limit the formation of the electric double layer. Accordingly, several groups reported

pore size effect in measured capacitance values (Simon *et al.* 2008, Raymundo–Pinero *et al.* 2006, Ghosh *et al.* 2012) and further models were developed (electric double–cylinder capacitor and electric wire–in–cylinder capacitor) to describe the modified electric double layer in mesoporous carbon and microporous carbon electrodes, respectively. (Huang *et al.* 2009)

In general, activated carbons (ACs), carbon nanotubes and graphene have been widely investigated for EDLC electrodes. (Ghosh *et al.* 2012, Zhang *et al.* 2009) To increase the exposed surface area of the electrode, different three–dimensional configurations of carbonaceous electrodes (templated carbon, (Lee *et al.* 1999, Ryoo *et al.* 2001) vertically aligned CNTs arrays (Talapatra *et al.* 2006, Halonen *et al.* 2013) and graphene–CNTs of a hierarchical structure (Du *et al.* 2011)) were developed to further improve the electric storage. It is worth mentioning that flexible and wear–resistant energy storage devices made of carbon electrodes are emerging.

Field emission electrodes represent another important potential application area of CNTs. (Rinzler *et al.*1995) Field emission is based on quantum tunneling of electrons that are ejected from a surface into a vacuum under the assistance of an applied electric field. The process is highly dependent on the work function of the material and on the shape (texture) of the cathode. In general, the Fowler–Nordheim equation $J=(A\beta^2E^2\Phi^{-1})exp(-B\Phi^{1.5}\beta^{-1}E^{-1})$ describes the process for bulk metals and other crystalline solids, where J is the emission current density, E is the applied field, A and B are constants, β is the field enhancement factor (the ratio of height over radius of curvature at the emission center), and Φ is the work function of the emitter. Thus, materials with low work function and elongated geometry and sharp tips or edges can greatly increase an emission current. Although the equation is very often used to model cold emission from CNT films and forests, it is worth noting that the field enhancement factors are much overestimated, and the linearized plots are not always linear because of the screening effects of nanotubes that are too close to each other. Nevertheless, nanotube forests and random films are indeed very promising materials for high current emission sources. By catalyst assisted CVD of CNTs, vertical arrays with different densities can be obtained on substrates, which is a very important process for practical utilization in flat panel displays (de Heer *et al.* 1995, Fan *et al.* 1999) or high frequency amplifiers. (Aleman *et al.* 2011)

3.2 Fabrication of three–dimensional carbonaceous electrodes

The synthesis process of three–dimensional carbonaceous electrodes combines two steps: stencil printing of the catalyst and the subsequent CVD process to grow nanostructured carbons. To prepare catalyst paste suitable for stencil printing, Raney® nickel 2400 slurry is mixed with poly(methyl methacrylate (PMMA) in 2–(2–butoxyethoxy) ethyl acetate and then processed in a ball–mill for ~15 hours. After the milling process, the paste was transferred from the ball–mill to a beaker by washing with small aliquots of acetone and then removed from the paste by heating to 90°C for about 15 minutes.

In the stencil printing process, laser cut stainless steel masks (thickness of 100 µm) having square patterns of 15×15 mm^2 size were used. The catalyst paste is doctored through the stencil with a lateral blade movement of ~1.0 $m{\cdot}s^{-1}$ speed. Si wafers with a 200 nm SiO_2 layer and polycrystalline alumina substrates were used. Before the stencil printing, Ti (40 nm) and Ni (100 nm) films were deposited on the substrates by e–beam evaporation and magnetron sputtering, respectively. The metallization layers are applied to improve adhesion of the catalyst on the substrates and to help electrical interfacing of the grown structures in subsequent experiments. The printed catalyst films were dried in a box furnace at 120°C in air for 15 minutes to remove the organic solvent. To reduce the catalyst, the patterned substrates were loaded in a cold–wall CVD reactor and heated to 400, 600 or 800°C (with a heating rate 100°C$\cdot min^{-1}$) in 500 sccm Ar and 50 sccm H_2 (5 mbar) and kept there for 30 minutes. After this step, C_2H_2 (acetylene) was introduced (flow rate of 10 sccm, at ~14 mbar) for a 20 minutes period to grow carbon and then the samples were cooled in a flow of Ar (500 sccm) and H_2 (50 sccm) (Fig. 1).

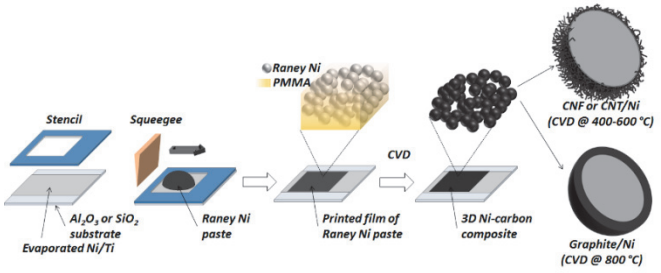

Fig. 1. Schematic drawing of the fabrication process including evaporation of under–metallization, stencil printing the catalyst and subsequent chemical vapor deposition of nanostructured carbons. (Paper I) Reproduced with the permission of The Royal Society of Chemistry, 2015.

3.3 Structural characterization of carbonaceous electrode grown at different temperatures

After the synthesis at 400°C, 600°C and 800°C, different kinds of carbonaceous structures formed and made nanocomposites with the Raney® Ni catalyst.(Fig. 2) Growth at 400°C or 600°C resulted in carbon filaments appearing on the surface of the catalyst, while at 800°C, much less filamentous products were observed.

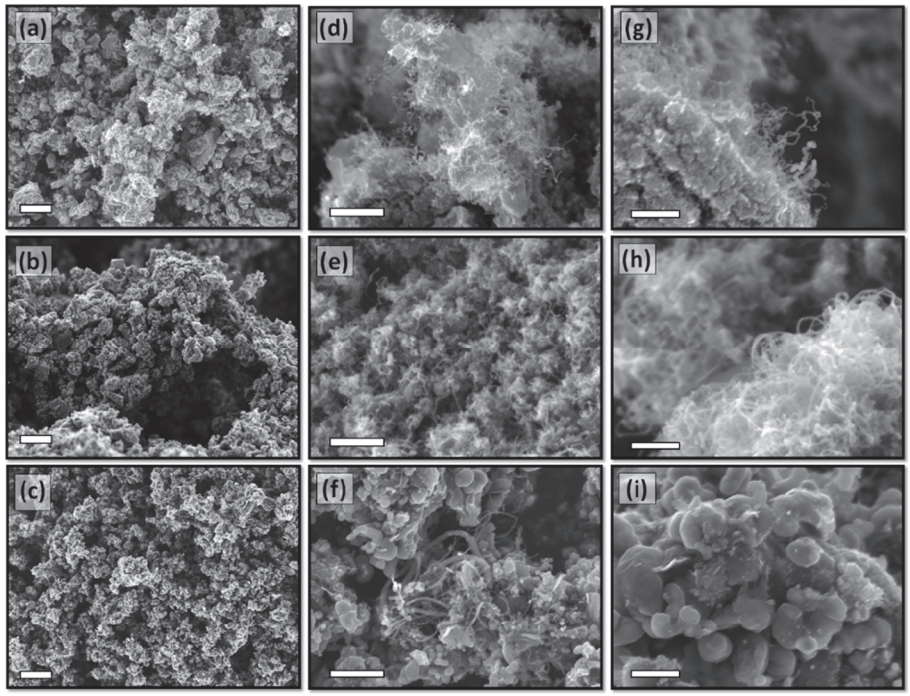

Fig. 2. SEM images of porous structure of carbon growth on nickel mesoporous layer at (a, d, g) 400°C, (b, e, h) 600°C, (c, f, i) 800°C. The scale bar of (a–c), (d–f) and (g–i) are 10 µm, 1 µm and 400 nm, respectively. (Paper I) Reproduced with the permission of The Royal Society of Chemistry, 2015.

According to TEM analysis, the majority of the filaments are multi–walled carbon nanotubes in these samples (Fig. 3). Besides nanotubes, also graphitic deposits of 40–50 nm thickness were found on the surface of the catalyst in the samples processed at 800°C. The growth mechanism on the porous Ni catalyst structure can be explained by the vapor–liquid–solid (VLS) growth model for carbon nanotubes on metal catalysts. First, the dissociation of hydrocarbon

molecules (to carbon atoms and clusters) is catalyzed at the Ni surface. After decomposition, the produced carbon species are adsorbed on and dissolved in the Ni particle. Since the precipitation of carbon is determined by the concentration and solubility of carbon in the metals, which highly depend on the surface curvature as well as on the temperature, even small fluctuations in such parameters can drive the carbon to phase separate and precipitate on the surface. (Halonen *et al.* 2008) The appearance of thick graphitic coating on the metal surface is attributed to a partial collapse of the mesoporous Ni structure, which is not favored to grow fibrous products. Furthermore, the quick precipitation of thick graphitic carbon layers on the surface is blocking (i.e. poisoning) the catalyst.

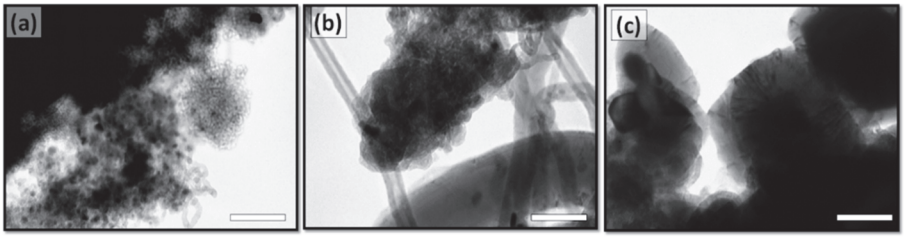

Fig. 3. TEM images of carbon structure on nickel mesoporous layers after (a) 400°C, (b) 600°C, and (c) 800°C growth. The scale bars show 50 nm. (Paper I) Reproduced with the permission of The Royal Society of Chemistry, 2015.

The production yield of carbon materials was elucidated by thermogravimetric analysis (TGA) (from 300°C to 800°C in air). The weight loss for the samples grown at 400°C, 600°C and 800°C was measured to be 29.0%, 48.0% and 36.0%, respectively. The results suggest the optimum temperature for carbon growth is at 600°C in good agreement with electron microscopy studies. The increased degradation temperature with the growth temperature of the composites is due to the better crystallinity of carbon deposits in the structures grown at higher temperatures (Fig. 4).

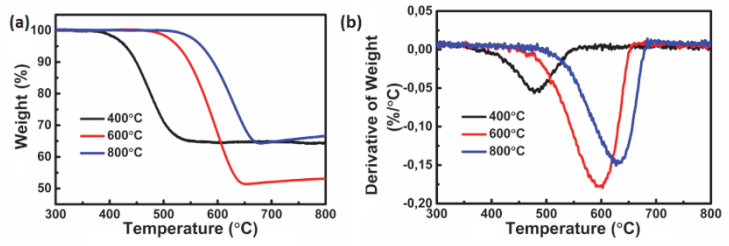

Fig. 4. (a) Weight and (b) differential thermal gravimetric curves for nanostructured Ni–carbon composites grown at different temperatures. (Paper I) Reproduced with the permission of The Royal Society of Chemistry, 2015.

On the other hand, the specific surface area of Raney nickel (100 $m^2 \cdot g^{-1}$) is decreased to approximately 65, 36 and 15 $m^2 \cdot g^{-1}$ after carbon growth in 400°C, 600°C and 800°C, respectively. The pore volume of the composites also varies with temperature (0.134 to 0.069 and 0.045 $mL \cdot g^{-1}$ for 400°C, 600°C and 800°C samples, respectively) (Fig. 5).

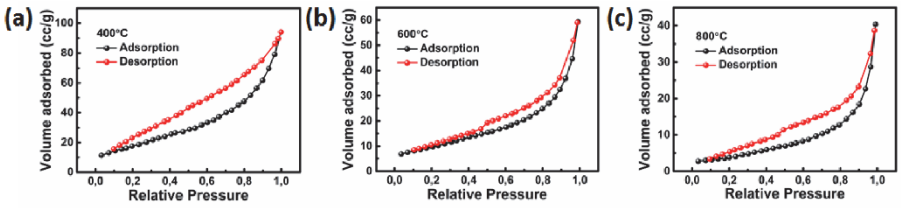

Fig. 5. Nitrogen adsorption and desorption isotherms for the carbon nanostructures grown on Raney nickel at (a) 400°C, (b) 600°C, and (c) 800°C. (Paper I) Reproduced with the permission of The Royal Society of Chemistry, 2015.

3.4 Applications in electric double–layer capacitors and cold emission electrodes

Cyclic voltammetry (CV) analysis (Fig. 6) of the composite films (sandwiching a cellulose separator) in aqueous KOH electrolytes show rather rectangular CV curves with large hysteresis loops in the applied voltage scan rate range (from 0.05 to 0.5 $V \cdot s^{-1}$), which is a good indication of ideal capacitor behavior. The specific capacitances are 12.3, 2.5 and 1.0 $F \cdot g^{-1}$ for the composites grown at 400°C, 600°C and 800°C, respectively. The decreased specific surface area of these electrodes can effectively explain the lowered capacitance with an increased growth temperature. The results measured for the 400°C samples are comparable with those reported for MWCNTs (18 $F \cdot g^{-1}$) (Talapatra *et al.* 2006) and (10–29 $F \cdot g^{-1}$)(Halonen *et al.* 2013) grown at much higher temperatures.

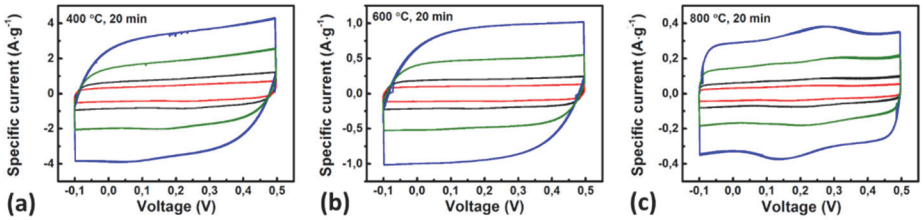

Fig. 6. Cyclic voltammetry curves with different charge/discharge rates of carbon grown on nickel mesoporous layer at (a) 400°C, (b) 600°C, and (c) 800°C. The red, black, green and blue curves correspond to charge/discharge rates of 0.05 $V \cdot s^{-1}$, 0.10 $V \cdot s^{-1}$, 0.25 $V \cdot s^{-1}$ and 0.50 $V \cdot s^{-1}$, respectively. (Paper I) Reproduced with the permission of The Royal Society of Chemistry, 2015.

The carbon/Raney® nickel composite electrodes also showed promising results in field emission experiments (Fig. 7) with turn–on fields below 0.9 $V \cdot \mu m^{-1}$. The results are comparable with those published for carbon nanobuds (0.65 $V \cdot \mu m^{-1}$), (Nasibulin *et al.* 2007), vertically aligned CNT arrays grown on Inconel (0.8–1.5 $V \cdot \mu m^{-1}$), (Sridhar *et al.* 2014) and significantly lower than that reported for screen printed carbon nanotubes (3 $V \cdot \mu m^{-1}$). (Li *et al.* 2003).

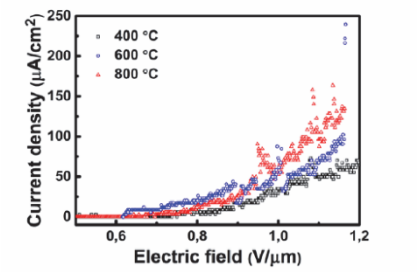

Fig. 7. Field emission of carbon/Raney nickel composites. (Paper I) Reproduced with the permission of The Royal Society of Chemistry, 2015.

4 Electrochemical detection of amines by trifluoroacetylazobenzene receptor molecules incorporated to Nafion® and CNT composites

In this chapter, the mechanism of amine sensing by trifluoroacetylazobenzene is discussed. The feasibility of the composites is evaluated in detecting four different amines using electrochemical measurements. The work is also complemented by optical measurements. These results are originally presented in Paper II.

4.1 Background

The approach of electrochemical sensing is associated with a direct conversion of the chemical information to electrical signal using transducers. The transducer (i.e. sensing element) is usually integrated with a specific recognition receptor to selectively correspond to a specific analyte. (Grieshaber *et al.* 2008) As the operation of electrochemical sensors is greatly influenced by the surface architectures that are in contact with the sensing element, sensing electrodes based on carbonaceous nanomaterials (e.g. CNTs and graphene) (Luong *et al.* 2005, Swamy *et al.* 2007) are considered as excellent candidates for such a purpose due to their high specific surface area, good electrical conductivity, and outstanding chemical stability. Cyclic voltammetry (CV) is the most common technique to obtain information about oxidation and reduction potentials as well as corresponding reaction mechanisms. In cyclic voltammetry, cyclic potential scans between working and counter electrodes are applied, while the current is monitored. Peaks in the acquired current–voltage plot indicate electron consumption/source corresponding to oxidation/reduction (at specific voltage values) of the given analyte.

4.2 Sensing mechanism of trifluoroacetylazobenze molecules to amine compounds

In this work, 4–(Dioctylamino)–4'–(trifluoroacetyl)azobenzene was applied in Nafion® and CNT–Nafion® composite films on the surface of glassy carbon electrodes to detect amine molecules (putrescine, cadevarine, ammonia) in solutions. This trifluoroacetylazobenze molecule was first synthesized by Mohr et al. and demonstrated as an optical amine sensor owing to the blue shift of its

absorption peak after binding with amines. As a strong electron acceptor, the trifluoroacetyl group of the dye forms a hemi–aminal group when reacting with amines. As a result of the reaction, the "box" of delocalized electrons shortens (Figure 8) (Mohr *et al.* 2004) and due to the stronger confinement, the resonance energy of the delocalized electrons increases and requires optical photons with a shorter wavelength to induce excitation/absorption.

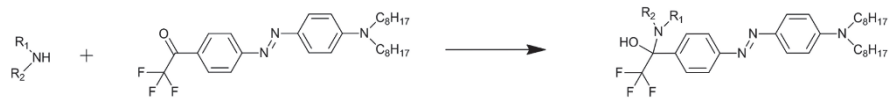

Fig. 8. Reaction of 4–(Dioctylamino)–4'–(trifluoroacetyl)azobenzene and amine. (Paper II) Reproduced with the permission of The Royal Society of Chemistry, 2015.

The receptor shows good optical response to mono– (ammonia and ethylamine) and diamines (putrescine and cadevarine) but fails when exposed to tetramethylammonium hydroxide because of the lacking dative electrons in the latter molecule. Another interesting feature of the receptor is the reversibility of optical response when removing the amine from its surrounding. This is caused by the reaction itself, which is an equilibrium process. The reverse reaction and thus reverse optical response are slow for diamines (Paper II). (Mertz *et al.*2003)

4.3 Electrochemical detection of amines using electrodes of receptor–Nafion® and receptor–CNT–Nafion® composites

Because of the reaction between trifluoroacetylazobenze and amines, we anticipate that receptor molecules adsorbed on the surface of electrodes can help detecting amines by means of electrical measurements. To verify our hypothesis, various types of composites using trifluoroacetylazobenze, carbon nanotubes and Nafion® were made and applied on the surface of glassy carbon electrodes to perform CV measurements in electrolytes with amines.

The receptor–CNT–Nafion® composites were made by dispersing 0.5 mg carboxyl functionalized CNTs in 1 mL Nafion® solution using ultrasonic agitation and then mixing 1 mL of the 4–(Dioctylamino)–4'–(trifluoroacetyl)azobenzene dye solution (1 mg·mL^{-1} in THF) while maintaining the ultrasonic treatment. The obtained dispersion was then drop–casted on a cleaned glassy carbon electrode (GCE, 3 mm in diameter). The surface was dried under ambient conditions and then used as a working electrode in a standard three–electrode cell setup with a Pt

counter electrode and Ag/AgCl reference electrode. The measurements were carried out at room temperature at 50 $mV \cdot s^{-1}$ sweeping rate using a potentistat (Princeton Applied Research VersaSTAT 3). Before each experiment, the electrolyte was purged with N_2 for 30 minutes.

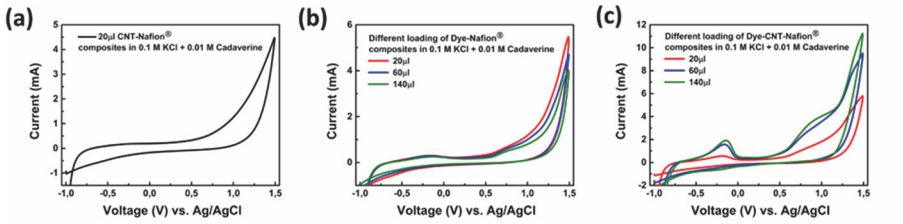

Fig. 9. Cyclic voltammetry curves of (a) Nafion®–CNT, (b) dye–Nafion® and (c) dye–Nafion®–CNT composites in 0.1 M KCl electrolyte in the presence of 0.01 M cadaverine. The plots with different colors compare the performance of composites with different amounts deposited on the glassy carbon electrode. The cycling speed used was 50 $mV \cdot s^{-1}$ and all the voltammograms shown are from the first cycle. (Paper II) Reproduced with the permission of The Royal Society of Chemistry, 2015.

The CNT–Nafion® modified electrode appears to be insensitive to cadaverine, while receptor–Nafion® modified electrode shows a small peak around -0.2 V (vs. Ag/AgCl) corresponding to the oxidation of the dye itself as well as a relative increase in the oxidation current around 0.8 V (vs. Ag/AgCl). On the other hand, in the case of the Receptor–Nafion®–CNT modified electrodes, there is a significant increase in the oxidation current around -0.2 V (vs. Ag/AgCl) in which a peak appears at around 0.8 V (vs. Ag/AgCl) (Fig. 9). The magnitudes of the currents for both peaks are increased as the amount of composite material is increased on the surface of glassy carbon electrode (Fig. 10). Based on the results, we may conclude that (i) the presence of receptor can promote oxidation of cadaverine, which takes place at around 0.8 V (vs. Ag/AgCl) and (ii) the presence of CNT network enhances the current response of the modified electrode, most likely by providing a large surface area for adsorption of cadaverine as well as by introducing a percolated electrical network for a more efficient charge transfer.

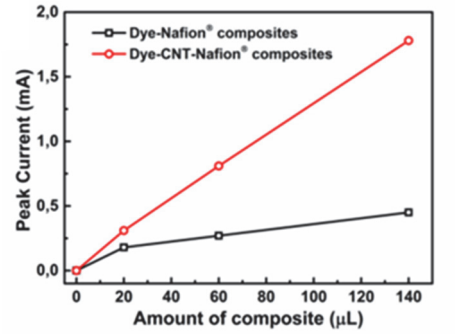

Fig. 10. Comparison of peak current corresponding to the electro–oxidation of cadaverine (Ep ~0.8 V (vs. Ag/AgCl) shown in Fig. 9 (b) and (c) after the background subtraction. (Paper II) Reproduced with the permission of The Royal Society of Chemistry, 2015.

Measurements carried out with other amines such as ammonia and putrescine as well as mixtures of ammonia putrescine and ammonia and cadevarine gave similar results as cadevarine only. Accordingly, the sensors are in general sensitive to amines but cannot differentiate between compounds.

5 Electrocatalytic performance of multi–walled carbon nanotubes decorated with copper and bimetallic CuPd nanoparticles in methanol electro–oxidation reactions

In this chapter, the principle of methanol electro–oxidation is described and the use of Cu and CuPd bimetallic particles grown on buckypapers as catalytic electrodes is discussed. The degradation of copper and bimetallic CuPd catalysts after cyclic potential scans in different electrolytes is also studied. These results are originally presented in Paper III.

5.1 Background

Nowadays, the ever increasing energy demand depends on fossil fuels, but its limited reserves drives us to look for sustainable solutions. Recently, fuel cells whose operation is based on the oxidation of small organic molecules on nanostructured catalytic electrodes has emerged owing to the convenient conversion of chemical energy to electricity. (Tian *et al.* 2007) Methanol is an excellent candidate for fuel, since it is easy to store and transport and it can be synthesized by a number of different chemical processes in extremely large quantities. Accordingly, direct oxidation of methanol in fuel cells has been widely investigated. (McNicol *et al.* 1999) The reaction of overall methanol oxidation can be divided by two half reactions at the anode and cathode:

$CH_3OH + H_2O \rightarrow CO_2 + 6H^+ + 6e^-$ (anode)

$1.5\ O_2 + 6H^+ + 6e^- \rightarrow 3\ H_2O$ (cathode)

$1.5\ O_2 + CH_3OH \rightarrow CO_2 + 2\ H_2O$ (overall reaction)

In general, platinum is the most often used and considered as the best catalyst in both anodes and cathodes. However, during the methanol oxidation, the carbon monoxide (CO) by–product may form and adsorb irreversibly on the surface of Pt thus poisoning it. (Aricò *et al.* 2001) PtRu (Alayoglu *et al.* 2008) and other Pt based bimetallic catalysts (Xu *et al.* 2009) have been proven to be robust enough against poisoning by carbon monoxide, however the price of Pt based catalysts is a major concern in practical applications. Although palladium based catalyst systems are not solving the major problems associated with price, abundance and sustainability, the relatively easy oxidation of Pd to PdO and its reduction back to metal is useful in many instances, since the catalyst can act as an oxygen reservoir in catalytic

processes. (Huber *et al.* 2006) Accordingly, Pd and bimetallic PdM (where M is a metal) catalyst are popular today for electrocatalytic oxidation reactions (Nitze *et al.* 2014; Chen *et al.* 2015; Ahmed *et al.* 2015; Bianchini *et al.* 2009). However, it is important to point out that in core–shell type catalysts, the amount of Pd may be significantly reduced compared to conventional nanoparticles without sacrificing the electrocatalytic behavior of the material. (Hu *et al.* 2014)

5.2 Copper and CuPd bimetallic catalysts decorated on MWCNTs buckypapers to form catalytic electrodes

Carbon nanotubes as large specific surface area and electrically conductive materials are commonly used as supporting materials in the configuration of catalytic anodes for fuel cells. To prepare buckypapers (thick films of randomly tangled CNTs) as growth templates for subsequent chemical plating and galvanic replacement, carboxylation (in cc. H_2SO_4/HNO_3 of 3:1 volume ratio) and palladium impregnation (from $C_6H_5CH_3$ solution of $Pd(acac)_2$ followed by calcination at 300°C in air and reduction at 500°C in 15% H_2/Ar) were first applied on MWCNTs (CVD grown, carbon > 95%; O.D. × L: 6–9 nm × 5 µm, Sigma–Aldrich) in solution phase. Subsequently, aqueous dispersions of Pd impregnated MWCNTs were made with the help of sodium dodecyl sulfate (SDS, 1 wt%) and deposited on cellulose nitrate membranes by the means of vacuum filtration to form Pd decorated buckypapers. This is followed by chemical plating of copper (reduction of copper–tartrate complex with formaldehyde) catalyzed by the Pd nanoparticles on the buckypapers as:

$$Cu^{2+} + 2HCOH + 4OH^- \rightarrow Cu + 2HCOO^- + H_2 + 2H_2O$$

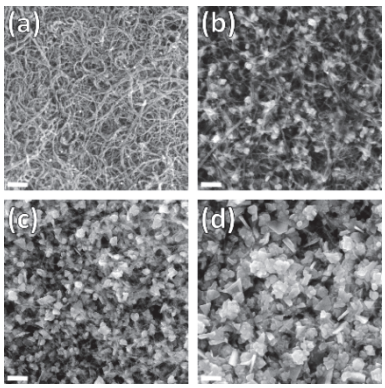

Fig. 11. Representative SEM images of a buckypaper surface (a) before and after (b) 2 minutes, (c) 4 minutes and (d) 8 minutes electroless plating in copper–tartrate bath. The scale bars show 200 nm. (Paper III)

After the plating process, the obtained copper nanoparticles were taken as sacrificial templates for partial replacement with palladium by simply submerging the Cu–buckypaper composites into a solution of K_2PdCl_4. Because the standard redox potential of $PdCl_4^{2-}$/Pd pair (0.59 V vs standard hydrogen electrode (SHE)) is higher than that of the Cu^{2+}/Cu pair (0.34 V vs SHE), the copper particles undergo a gradual oxidation and dissolution while palladium ions are reduced and replace copper, resulting in the formation of hollow nanocages as shown in the inset of Fig. 12 (a). The overall reaction is spontaneous and can be written as $Cu(s) + Pd^{2+}(aq) \rightarrow Pd(s) + Cu^{2+}(aq)$. (Mohl *et al.* 2011)

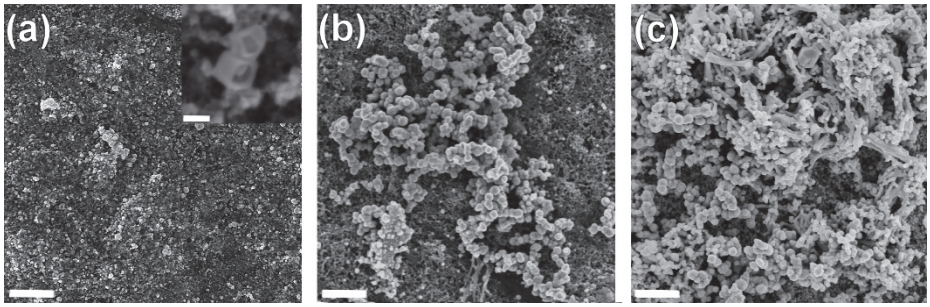

Fig. 12. SEM images of CuPd bimetallic structures after (a) 2 minutes, (b) 60 minutes and (c) 960 minutes replacing reaction. The scale bars show 1 µm. Inset of (a): enlarged image showing hollow nanocages. The scale bar is 100 nm. (Paper III)

The transmission electron micrographs demonstrate that the deposited copper is rapidly oxidized to cuprous oxide (Cu_2O) after the reaction, as the observed lattice fringes with d–spacing of 0.25 nm and 0.30 nm can be assigned to the (111) and (101) planes of Cu_2O (Fig. 13 (a–c)). However, in the case of the bimetallic catalyst materials, the appearance of tiny crystals (~5 nm in diameter) with lattice fringes of approximately 0.23 nm spacing correspond to Pd (111) indicating that Pd is in its metallic form (Fig. 13 (d–l)).

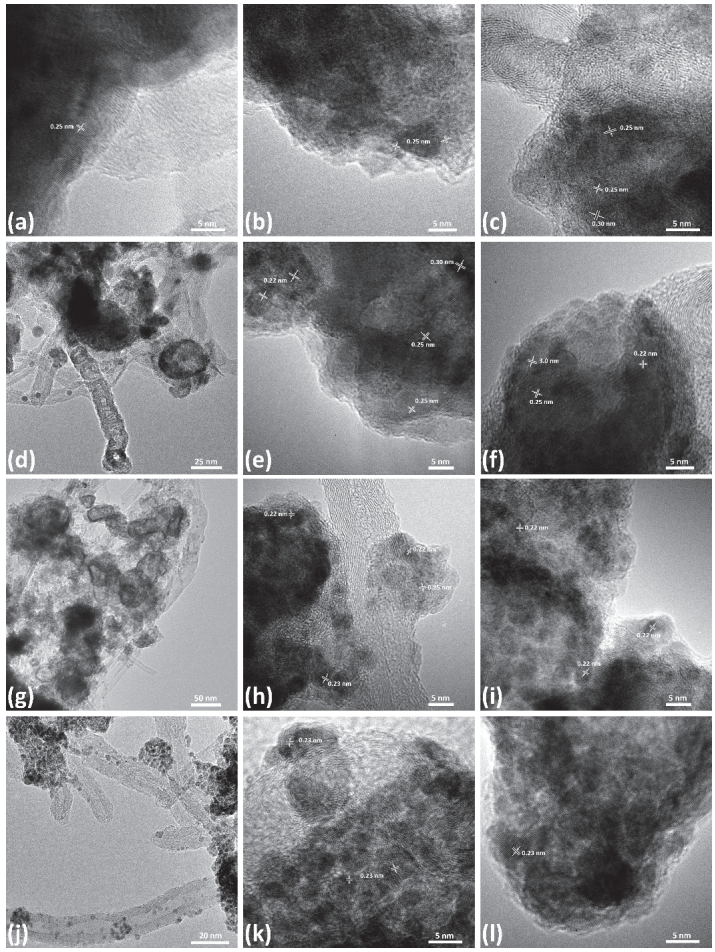

Fig. 13. HR–TEM images of (a–c) 2 minutes–plating copper, (d–f) 2 minutes, (g–i) 60 minutes and (j–l) 960 minutes replaced CuPd. (Paper III)

5.3 Electrocatalytic performance of copper and CuPd bimetallic catalysts decorated on MWCNTs network electrode in electro–oxidation of methanol

Since copper may be in a number of different oxidation states, the reference voltammogram was first measured in 1.0 M KOH electrolyte to clarify the working potential of the corresponding redox reaction. In Figure 14 (a), the main anodic peak at -100 mV can be assigned to Cu(0)/Cu(II) and Cu(I)/Cu(II) transition through $Cu(OH)_2$ formation from the metal and cuprous oxide, respectively.

There are two minor anodic peaks appearing between 0.4 V and 0.7 V as shown in the inset of Fig. 17 (a). Peak 1 is due to the oxidation of copper in alkaline media ($Cu + 3OH^- \rightarrow HCuO_2^- + H_2O + 2e^-$), while peak 2 is assigned for the Cu(II) to Cu(III) oxidation. (Shames El Din *et al.* 1964, Heli *et al.* 2004)

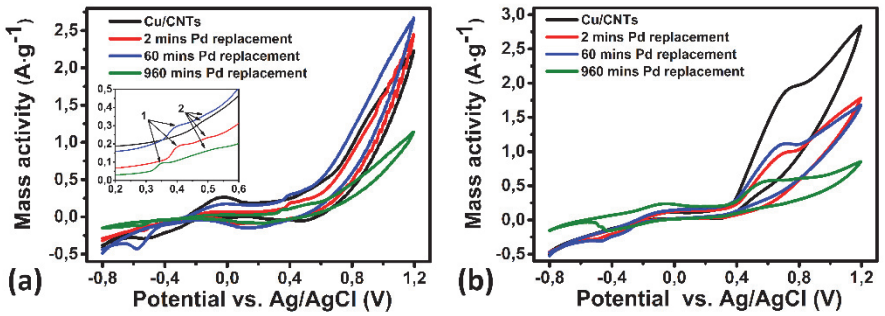

Fig. 14. Cyclic voltammetry curves of Cu or CuPd/buckypaper composites in (a) 1 M KOH solution and (b) 1 M KOH solution containing 1 M methanol. Inset of (a): enlarged plot of (a) at potential range between 0.2–0.8 V vs. Ag/AgCl. (Paper III)

Oxide–mediated electro–oxidation of alcohols and amines on catalytic surfaces of non–noble transition metals such as copper has been studied in detail. (Fleischmann *et al.* 1972) Being a strong oxidizing species for methanol, Cu(III) further ensures the electrocatalytic activity of copper in the Cu–containing electrodes. On the other hand, Fig. 17 (b) suggests the electrocatalytic oxidation of methanol on copper and different CuPd bimetallic catalysts takes place separately on the two different metals (between 0.6 V – 0.8 V on copper catalyst (Heli *et al.* 2004) and between -0.2 V – 0 V on palladium catalyst (Shih *et al.* 2013)). Considering the atomic composition of copper and palladium in the three different CuPd bimetallic structures, it seems copper is the dominant catalyst in the process

no matter what the palladium concentration is in the corresponding bimetallic structure (even as high as 80 at% for 960 minutes replaced CuPd sample). This copper dominant behavior may be attributed to the presence of oxide phases (palladium oxide and cuprous oxide) in CuPd/buckypaper composites. The appearance of oxide after the galvanic replacement results in a decreased catalytic activity of the electrodes. Moreover, the oxidation of copper to cuprous oxide in the structure also contributes to the limited charge transfer caused by the relatively low conductivity of the oxide compared to the pure metal, and because of the formation of non–ohmic interfaces between the metals and semiconducting oxide phases.

5.4 Degradation and durability of copper and CuPd bimetallic catalysts decorated on MWCNTs network electrode in the electro–oxidation of methanol

The degradation of copper or CuPd/buckypaper composites in 1.0 M KOH with the absence/presence of methanol was also studied. In the case of copper decorated CNTs, crystalline $Cu(OH)_2$ with needle shape structures was formed in KOH electrolyte. However, the acicular features associated with anodized copper are not visible for the other three CuPd bimetallic structures meaning that palladium can efficiently prevent copper from anodic oxidation. In addition, the intact hollow nanocages further prove that even small amounts of palladium could also provide great protection for the CuPd bimetallic structure from the corrosion during the cycling treatment in the alkaline solution.

On the other hand, in the presence of methanol (1.0 M methanol and 1.0 M KOH), after 5 electrocatalytic cycles, the morphology of the four composites are significantly changed. In the Cu–buckypaper composite, the deposited copper particles are nearly absent from the surface, while in the case of the CuPd–buckypaper composites a thick poorly conducting phase was observed in the samples by SEM.

Chronoamperometry measurements (Fig. 15) were performed to assess the durability of the catalytic electrodes in 1.0 M methanol in 1.0 M KOH electrolyte at the oxidation potential of copper (0.72 V versus to Ag/AgCl electrode). The polarization current rapidly and considerably dropped after the start of the measurement, however after ~15 min the current is settled to fairly constant values. The sudden loss of conductivity for the Cu and CuPd/buckypaper composites may be explained by the rapid oxidation of copper in alkaline solution. The decrease of

the current in the chronoamperometry curves seems to correlate with the atomic composition of the catalyst metals. Electrodes with large Pd content show better current stability, which is in agreement with our previous claim that palladium in CuPd bimetallic structures can protect copper from oxidation.

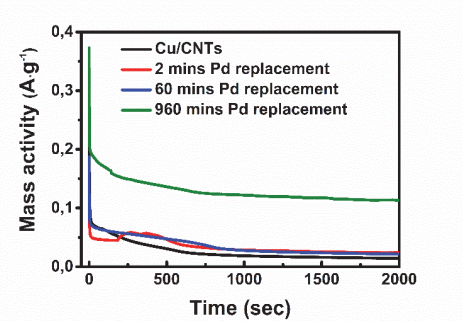

Fig. 15. Chronoamperometric curves of Cu or CuPd/buckypaper composites in 1 M KOH solution containing 1 M methanol at fixed potential of 0.72 V versus Ag/AgCl reference electrode. The mass activity is the current normalized to the total mass of the electrode material (i.e. carbon together with the metals as determined by weight measurements of the samples). (Paper III)

It is worth mentioning that the generally higher mass activity measured for the *960 min Pd replacement* electrocatalyst in the chronoamperometric data reflects well the superior stability of the material compared to the other samples. This is particularly important by considering the originally higher mass activity of the other samples as measured in the first voltammogram cycle for the *Cu/CNT, 2 min Pd and 60 min Pd replacement* samples shown in Figure 14(b).

6 CNT forests as growth templates for capping tungsten carbide and tungsten disulfide catalytic electrodes in the hydrogen evolution reaction

In this chapter, the hydrogen evolution reaction and the role of catalysts in the electrochemical process are introduced. This is followed by a description of a novel approach to produce catalytic composite electrodes of tungsten carbide and tungsten disulfide with CNT forests. The electrocatalytic performance of the new composites is evaluated in the hydrogen evolution reaction. The results are originally presented in Paper VI.

6.1 Background

Water splitting ($H_2O \rightarrow H_2 + 0.5O_2$) to produce H_2 is an important reaction as it can supply clean fuel with zero pollution. Water splitting is achieved by two main approaches: electrolysis and photolysis. The reaction requires an input energy of $\Delta G = 237.1$ kJ·mol^{-1} at standard conditions, which corresponds to a thermodynamic voltage of 1.23 V. (Walter *et al.* 2010) The overall reaction can be separated to cathodic ($2H^+ + 2e^- \rightarrow H_2$) and anodic ($H_2O \rightarrow 0.5O_2 + 2H^+ + 2e^-$) sub–reactions referred to as H_2 and O_2 evolution reactions, respectively. For the H_2 evolution reaction, two different reaction routes i.e. the Volmer–Heyrovsky and Volmer–Tafel mechanisms are used to describe the process. In both models, surface adsorbed H atoms (Volmer step) are considered as intermediates in the formation of molecular H_2, thus the free energy of hydrogen adsorption (ΔG_H) greatly influences the overall reaction rate. The best catalyst would have the ΔG_H value close to zero since higher or lower values would limit the subsequent Heyrovsky or Tafel step and thus lower the efficiency of hydrogen production. This principle derives the well–known volcano plot, in which the catalytic activity of a material for the HER is plotted as a function of the hydrogen–metal bond strength. (Greeley *et al.* 2006) Among the catalysts studied, platinum and other noble analogues are performing the best. However their price and limited availability greatly restricts large–scale applications in practice just like in fuel cell applications as mentioned in the previous chapter.

Recently, carbides (Levy *et al.* 1973) and dichalcogenides (Sobczynski *et al.* 1988) of the group six transition–metals (Cr, Mo, W) have become popular subjects of study in the fields of catalysts and energy applications. Particular interest

towards tungsten monocarbide (WC) is shown for its catalytic similarity to platinum group metals. (Ji *et al.* 2008, Gosselink *et al.* 2013, Garcia–Esparza *et al.* 2013, Hurt *et al.* 2014) The chemical similarity of tungsten monocarbide is partially attributed to the intercalation of carbon atoms to the tungsten lattice, which induces a "platinum–like" d–band in the electronic density of states. (Bennett *et al.* 1974) By using WC as a host material with a very thin Pt coating layer, the Pt–WC composites can reach similar catalytic performance to Pt. On the other hand, the bulk dichalcogenides such as MoS_2 and WS_2 were first suggested as inactive in H_2 evolution (Tributsch *et al.* 1977) due to its semiconducting 2H phase. (Voiry *et al.* 2013, Morales–Guio *et al.* 2014, Lukowski *et al.* 2014) However, nanostructured sulfides show significant catalytic activity compared to their bulk materials owing to the metal rich edge area (Hinnemann *et al.* 2005) in the lamellar structure and also most likely because of the presence of the metallic 1T phase. (Voiry *et al.* 2013) Accordingly, the lamellar nanostructures of MoS_2 and WS_2 are expected to have improved catalytic efficiency when growing them on curved and rough substrates while maintaining the perpendicular orientation of nanoflakes (instead of parallel lapping on the surface). (Wang *et al.* 2013)

6.2 Direct growth of WC and WS_2 on CNT forests and the structural characterization

For the growth of WC and WS_2 on CNTs, a thin layer of tungsten (150 nm) is first deposited on the top surface of the cleaned nanotube forests. Accordingly, the obtained composites would also be in the top–most region of the nanotube films after carburization or sulfurization (Fig. 16).

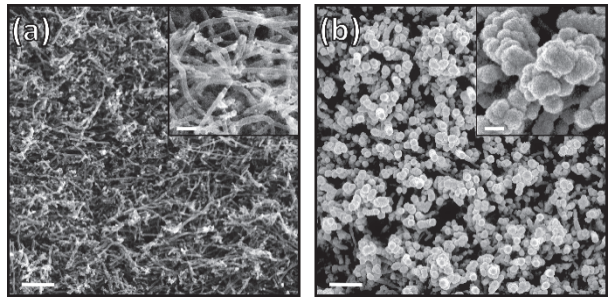

Fig. 16. SEM images of (a) the top surface of a CNT forests after annealing in air and cleaning with Scotch–tape peeling and (b) the tungsten coated CNT forest (CNT–W).

The scale bars show 1 μm (main panels) and 200 nm (insets). (Paper IV) Reproduced with the permission of The Royal Society of Chemistry, 2015.

Upon carburization, the distortion of the tungsten crystal lattice due to the diffused carbon atoms is observed in a series of shifted diffraction peaks in the XRD patterns (Fig. 17 (a)). As the annealing time was extended from 1 to 4 hours at 1000°C, three primary diffraction peaks of hexagonal tungsten monocarbide (WC) appear, indicating that tungsten is partly converted to carbide. On the other hand, sulfurization easily transforms W to WS_2 already at 800°C (Fig. 17(b)). The enhanced intensity of diffraction peaks for the samples obtained at higher temperatures are explained by the enlargement of crystalline size and improved crystallinity.

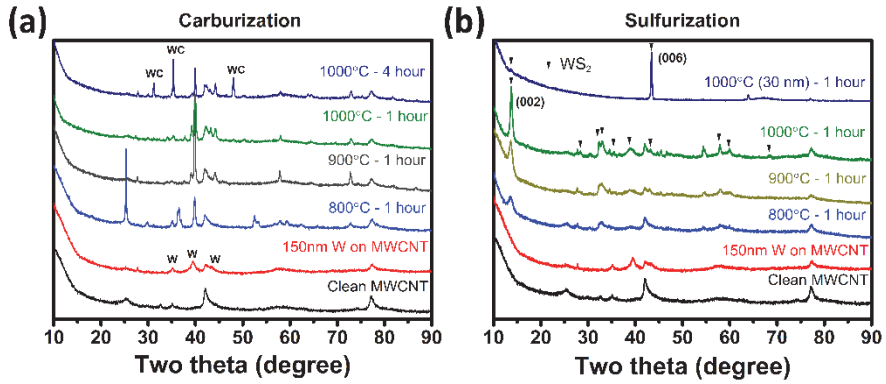

Fig. 17. X–ray diffraction spectra of clean CNT array, CNT–W composite, and produced composites after (a) carburization and (b) sulfurization. (Paper IV) Reproduced with the permission of The Royal Society of Chemistry, 2015.

The surface morphology of deposited W smoothens with increasing temperature in Ar atmosphere (Fig. 18(a–d)). The gradual diffusion and incorporation of carbon atoms into the lattice of tungsten lattices and the induced WC formation can explain such a change since melting of tungsten nanostructures is not possible at the temperatures applied. The change of the morphology during sulfurization is more dramatic. The W layer is becoming fine–structured already at 800°C and 900°C, while increasing the temperature of sulfurization to 1000°C results in an edge–on lamella structure of WS_2 along each carbon nanotube (Fig. 18(e–g)). To increase the surface area and reduce the size of WS_2 basal plane without sacrificing the edge–on lamella structure on CNTs array, the deposition

thickness of tungsten was decreased from 150 nm to 30 nm and employed the same sulfurization process as earlier (1000°C for 1 hour). As shown in Fig. 18 (h), the WS_2 crystals are split into nanoflakes that are well–dispersed and separated on the CNTs.

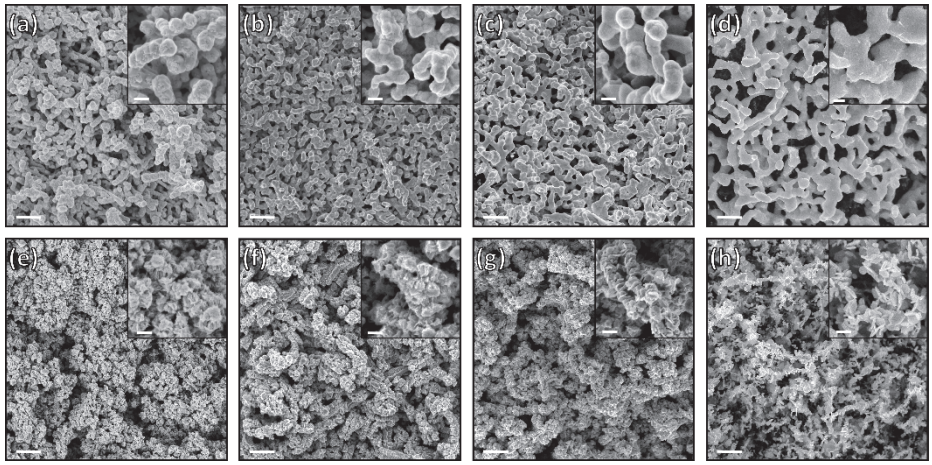

Fig. 18. Scanning electron micrographs of CNT–WC composites after carburization of CNT–W (150 nm W) at (a) 800°C, (b) 900°C, (c) 1000°C for 1hour and (d) at 1000°C for 4 hours. CNT–WS_2 composites synthesized at (d) 800°C, (e) 900°C, (f) 1000°C for 1hour. (h) CNT–WS_2 composite after sulfurization of CNT–W (30 nm W) at 1000°C for 1hour. The scale bars denote 1 μm in the main panels and 200 nm in the insets. (Paper IV) Reproduced with the permission of The Royal Society of Chemistry, 2015.

High–resolution transmission electron micrographs of the 4 h annealed CNT–WC samples shows CNT–like structures embedded in the host material (Fig. 19 (a)). The lattice spacing measured for the matrix (~3.0 Å) may correspond to the (001) planes of the hexagonal WC (2.84 Å) in agreement with the XRD measurements. However, it is worth mentioning that the (100) spacing of cubic W is also rather close (3.16 Å) to the measured ~3.0 Å value. On the other hand, the embedded CNT–like structures have a lattice parameter of ~3.6 Å suggesting strain in the [002] direction of the CNT walls or graphitic flakes (original d–spacing is 3.4 Å). In the case of the CNT–WS_2 samples, highly crystalline WS_2 was obtained after sulfurization (Fig. 19(b)). Layered hexagonal nanoflake structures with a typical thickness of 10–15 nm and diameter of up to ~200 nm are observed around the nanotubes. The gap between fringes is 0.62 nm, which corresponds to the d–spacing of WS_2 (002) plane (6.3 Å).

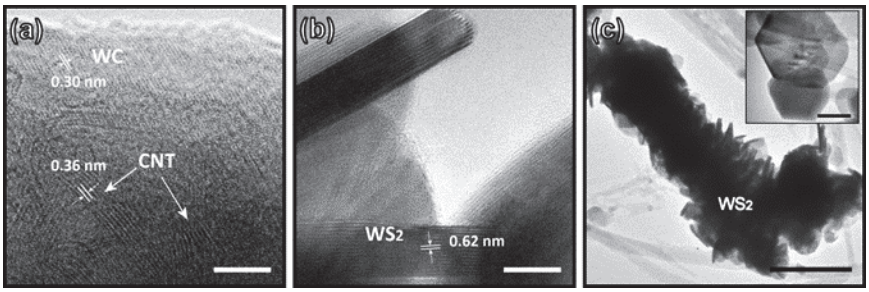

Fig. 19. High–resolution TEM images of W–CNT composites after (a) carburization at 1000°C for 4 hours; scale bar is 5 nm and (b) sulfurization at 1000°C for 1 hour; scale bar is 10 nm. (c) WS2 nanoflakes around a CNT; scale bar is 400 nm. Inset shows individual nanoflakes; scale bar is 50 nm. (Paper IV) Reproduced with the permission of The Royal Society of Chemistry, 2015.

6.3 Electrocatalytic performance of CNT–WC and CNT–WS_2 in hydrogen evolution reaction

After solder mounting the samples (i.e. CNT, CNT–W, CNT–WC and CNT–WS_2) on bronze cantilevers to make working electrodes for electrochemical measurements, the structures were analyzed in a three–electrode arrangement in 0.05 M H_2SO_4 with glassy carbon and silver chloride (Ag/AgCl) as counter and reference electrodes, respectively. In the hydrogen evolution reaction, an overpotential of 435 mV (the potential at a current density of 10 $mA \cdot cm^{-2}$) is observed for the W–CNT composite, whereas it is 165 mV for the Pt wire in good agreement with their free energy for hydrogen adsorption (ΔG_H). (Greeley *et al.* 2006) The behavior of the WC–CNTs electrode is quite similar to that of the W–CNT, which is probably due to the large amount of unreacted W on the nanotubes (Fig. 6(a)). The corresponding Tafel slopes (Fig. 20(b)) are 103 $mV \cdot dec^{-1}$ and 122 $mV \cdot dec^{-1}$ for CNT–W and CNT–WC composites, respectively. On the other hand, the limited catalytic activity of the CNT–WS_2 samples is most likely due to the presence of 2H phase (the W atom is coordinated by 6 S atoms in a trigonal prismatic arrangement) rather than catalytically active 1T phase (W is in an octahedral coordination with surrounding S atoms resulting in a strained structure) in the samples, (Voiry *et al.* 2013) which is caused by the high reaction temperature (1000°C). The Tafel slopes of CNT–WS_2 composites (182 $mV \cdot dec^{-1}$ and 159 $mV \cdot dec^{-1}$) also support our assumption that our nanoflakes are in the less conductive 2H WS_2 form. It is important to mention that the overpotential (684 mV)

of the porous structure is much lower than that of bulk 2H WS_2 (over 1 V). The good and thin electrical interface (CNT–WS_2–electrolyte) in the samples caused by the direct growth of the edge–on lamellae can reasonably explain the lower overpotential. (Voiry *et al.* 2013)

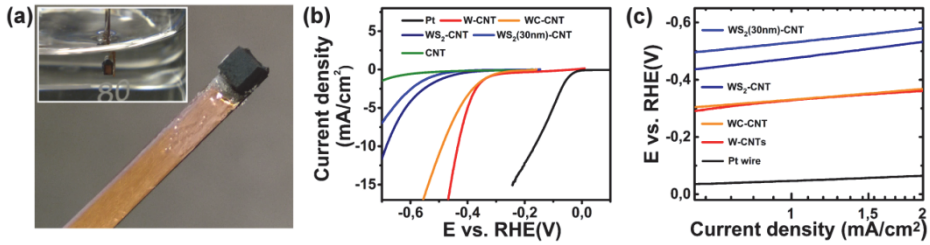

Fig. 20. (a) Camera image of a solder mounted electrode with a CNT forest foot print size of 2×2 mm^2. Inset shows an electrode in operation. (b) Linear sweep voltammograms of different CNT based composites electrodes at their corresponding active potential region of hydrogen evolution reaction in 0.05 M H_2SO_4 solution (scan rate 10 $mV \cdot s^{-1}$). (c) Tafel plot of the corresponding voltammograms. (Paper IV) Reproduced with the permission of The Royal Society of Chemistry, 2015.

7 Summary and conclusions

Carbon nanotubes have been proven as multifunctional materials in the past two decades owing to their unique set of properties such as high specific surface area, good electrical and thermal conductivity, great mechanical strength, light weight and chemical inertness. Besides these features, after chemical functionalization, incorporation of polymers or surfactants, the nanotubes can also fit fabrication processes in solution phase broadening the spectrum of their utilization even further. The integration of functional CNTs with different active materials provides a versatile strategy for innovations and solving technical challenges.

Multi–dimensional carbon based nanostructures have been studied in this thesis for electrode applications. The porous and electrically conductive architecture with large permeable surface area can accommodate high loading amounts of active materials. Based on this principle, the direct growth of active materials on carbon template has emerged lately which ensures the intimate interface between the carbon host and the capping materials with good electrical and mechanical interface.

The synthesis of three–dimensional carbon–metal electrodes through the CVD of filamentary carbons on printed porous catalyst structure has been demonstrated as a facile approach to obtain electrode structures on solid surfaces (Paper I). The novel integrated electrodes show comparable performance in EDLC and field–emission applications with other CNT based electrodes. The method may be optimized further by using smaller catalyst particles and other printing techniques to compose growth templates with a better print resolution and higher porosity.

CNTs incorporated into organic composites via solution phase processing displayed better response in electrochemical sensing than the reference materials without nanotubes (Paper II). The methodology of simply mixing CNTs with active materials in dispersions is expected to fit roll–to–roll fabrication processes allowing even large–scale production of low–cost sensing devices.

Chemical template growth of catalyst nanoparticles on two–dimensional random networks of carbon nanotubes (Paper III) as well as on three–dimensional vertically aligned CNT forest (Paper IV) have been developed and studied for electrocatalytic electrodes. Oxidation of methanol and production of H_2 from water were demonstrated.

The versatility of materials combinations and the feasibility of using the conductive and porous CNT scaffolds have been proven to offer a facile technique to fabricate novel electrodes for a number of different applications.

References

Adams GB, O'Keeffe M & Ruoff RS (1994) Van Der Waals Surface Areas and Volumes of Fullerenes. The Journal of Physical Chemistry 98 (38): 9465–9469.

Ahmed MS & Jeon S (2015) Electrochemical activity evaluation of chemically damaged carbon nanotube with palladium nanoparticles for ethanol oxidation. Journal of Power Sources 282: 479–488.

Ajiki H. & Ando T (1993) Electronic states of carbon nanotubes Journal of the Physical Society of Japan 62(4): 1255–1266.

Alayoglu S, Nilekar AU, Mavrikakis M & Eichhorn B (2008) Ru–Pt core–shell nanoparticles for preferential oxidation of carbon monoxide in hydrogen. Nature Materials 7(4): 333–338.

Alemán BJ, Sussman A, Mickelson W & Zettl A (2011) A carbon nanotube–based NEMS parametric amplifier for enhanced radio wave detection and electronic signal amplification. Journal of Physics: Conference Series 302: 012001.

Anthopoulos TD, Singh B, Marjanovic N, Sariciftci NS, Ramil AM, Sitter H, Cölle M & de Leeuw DM (2006) High performance n–channel organic field–effect transistors and ring oscillators based on C60 fullerene films. Apply Physics Letter 89(21): 213504.

Aricò AS, Srinivasan S & Antonucci V (2001) DMFCs: from fundamental aspects to technology development. Fuel Cells 1(2): 133–161.

Arnold MS, Green AA, Hulvat JF, Stupp SI & Hersam MC (2006) Sorting carbon nanotubes by electronic structure using density differentiation. Nature Nanotechnology 1(1): 60–65.

Awasthi S, Awasthi K, Kumar R & Srivastava ON (2009) Functionalization effects on the electrical properties of multi–walled carbon nanotube–polyacrylamide composites. Journal of Nanoscience and Nanotechnology 9(9):5455–5460.

Bae S, Kim H, Lee Y, Xu X, Park JS, Zheng Y, Balakrishnan J, Lei T, Kim HR, Song YI, Kim YJ, Kim KS, Özyilmaz B, Ahn JH, Hong BH & Iijima S (2010) Roll–to–roll production of 30–inch graphene films for transparent electrodes. Nature Nanotechnology 5(8): 574–578.

Baker RTK, Barber MA, Harris PS, Feates FS & Waite RJ (1972) Nucleation and growth of carbon deposits from the nickel catalyzed decomposition of acetylene. Journal of Catalysis 26(1): 51–62.

Bennett LH, Cuthill JR, McAlister AJ, Erickson NE & Watson RE (1974) Electronic structure and catalytic behavior of tungsten carbide. Science 184(4136): 563–565.

Bianchini C & Shen PK (2009) Palladium–based electrocatalysts for alcohol oxidation in half cells and in direct alcohol fuel cells. Chemical Reviews 109(9): 4183–4206.

Bolotin KI, Sikes KJ, Jiang Z, Klima M, Fudenberg G, Hone J, Kim P & Stormer HL (2008) Ultrahigh electron mobility in suspended graphene. Solid State Communications 146(9–10): 351–355.

Bourlon B, Miko C, Forró L, Glattli DC & Bachtold A (2004) Determination of the intershell conductance in multiwalled carbon nanotubes. Physical Review Letters 93(17) 176806.

Cao X, Shi Y, Shi W, Lu G, Huang X, Yan Q, Zhang Q & Zhang H (2011) Preparation of novel 3D graphene networks for supercapacitor applications. Small 7(22): 3163–3168.
Chen J, Hamon MA, Hu H, Chen YS, Rao AM, Eklund PC & Haddon RC (1998) Solution properties of single–walled carbon nanotubes. Science 282(5386): 95–98.
Chen J, Liu HY, Weimer WA, Halls MD, Waldeck DH & Walker GC (2002) Noncovalent engineering of carbon nanotube surfaces by rigid, functional conjugated polymers. Journal of the American Chemical Society 124(31): 9034–9035.
Chen QS, Xu ZN, Peng SY, Chen YM, Lv DM, Wang ZQ, Sun J & Guo GC (2015) One–step electrochemical synthesis of preferentially oriented (111) Pd nanocrystals supported on graphene nanoplatelets for formic acid electrooxidation. Journal of Power Sources 282: 471–478.
Chen T, Wang S, Yang Z, Feng Q, Sun X, Li L, Wang ZS & Peng H (2011) Flexible, light–weight, ultrastrong, and semiconductive carbon nanotube fibers for a highly efficient solar cell. Angewandte Chemie International Edition 50(8): 1815–1819.
Chen W & Yan L (2011) In–situ self–assembly of mild chemical reduction graphene for three–dimensional architectures. Nanoscale 3(8): 3132–3137.
Chen Y, Zhang Y, Hu Y, Kang L, Zhang S, Xie H, Liu D, Zhao Q, Li Q & Zhang J (2014) State of the art of single–walled carbon nanotube synthesis on surfaces. Advanced Materials 26(34): 5898–5922.
Chowalla M, Teo KBK, Ducati C, Rupersinghe NL, Amaratunga GAJ, Ferrari AC, Roy D, Robertson J & Milne WI (2001) Growth process conditions of vertically aligned carbon nanotubes using plasma enhanced chemical vapor deposition. Journal of Applied Physics 90(10): 5308–5317.
Coleman JN, Khan U & Gun'ko YK (2006) Mechanical reinforcement of polymers using carbon nanotubes. Advanced Materials 18(6): 689–706.
Correa–Duarte MA, Wagner N, Rojas–Chapana J, Morsczeck C, Thie M & Giersig M (2004) Fabrication and biocompatibility of carbon nanotube–based 3D networks as scaffolds for cell seeding and growth. Nano Letters 4(11): 2233–2236.
Cumings J & Zettl (2000) A low–friction nanoscale linear bearing realized from multiwall carbon nanotubes. Science 289(5479):602–604.
Dalton AB, Collins S, Muñoz E, Razal JM, Ebron VH, Ferraris JP, Coleman JN, Kim BG & Baughman RH (2003) Super–tough carbon–nanotube fibres. Nature 2003, 423(6941), 703.
de Heer WA, Châtelain A & Ugarte D (1995) A carbon nanotube field–emission electron source. Science 270(5239): 1179–1180.
De Jong KP & Geus JW (2000) Carbon nanofibers: catalytic synthesis and applications. Catalysis Reviews: Science and Engineering 42(4): 481–510.
Du F, Yu D, Dai L, Ganguli S, Varshney V & Roy AK (2011) Preparation of tunable 3D pillared carbon nanotube–graphene networks for high–performance capacitance. Chemistry of Materials 23(21): 4810–4816.
Durkop T, Getty SA, Cobas E & Fuhrer MS (2004) Exraordinary mobility in semiconducting carbon nanotubes. Nano Letters 1(4): 35–39.

Ebbesen TW, Lezec HJ, Hiura H, Bennett JW, Ghaemi HF & Thio T (1996) Electrical conductivity of individual carbon nanotubes. Nature 382(6586): 54–56.

Eda G, Fanchini G & Chhowalla M (2008) Large–area ultrathin films of reduced graphene oxide as a transparent and flexible electronic material. Nature Nanotechnology 3(5): 270–274.

El–Kady MF, Strong V, Dubin S & Kaner RB (2012) Laser scribing of high–performance and flexible graphene–based electrochemical capacitors. Science 335(6074): 1326–1330.

Ericson LM, Fan H, Peng H, Davis VA, Zhou W, Sulpizio J, Wang Y, Booker R, Vavro J, Guthy C, Parra–Vasquez ANG, Kim MJ, Ramesh S, Saini RK, Kittrell C, Lavin G, Schmidt H, Adams WW, Billups WE, Pasquali M, Hwang WF, Hauge RH, Fischer JE & Smalley RE (2004) Macroscopic, neat, single–walled carbon nanotube fibers. Science 305(5689): 1447–1450.

Espinosa HD, Filleter T & Naraghi M (2013) Multiscale experimental mechanics of hierarchical carbon–based materials. Advanced Materials 24(21): 2805–2823.

Falvo MR, Clary GJ, Taylor RM, Chi V, Brooks Jr FP, Washburn S & Superfine R (1997) Bending and buckling of carbon nanotubes under large strain, Nature 389(6651): 582–584.

Fan S, Chapline MG, Franklin NR, Tombler TW, Cassell AM & Dai H (1999) Self–oriented regular arrays of carbon nanotubes and their field emission properties. Science 283(5401): 512–514.

Fan Z, Yan J, Zhi L, Zhang Q, Wei T, Feng J, Zhang M, Qian W & Wei F (2010) A three–dimensional carbon nanotube/graphene sandwich and Its application as electrode in supercapacitors. Advanced Materials 22(33): 3723–3728.

Férey G & Cheetham AK (1999) Prospects for Giant Pores, Science 283(5405): 1125–1126.

Fleischmann M, Korinek K & Pletcher D (1972) The kinetics and mechanism of the oxidation of amines and alcohols at oxide–covered nickel, silver, copper, and cobalt electrodes. Journal of the Chemical Society, Perkin Transactions 2 10:1396–1403.

Foroughi J, Spinks GM, Wallace GG, Oh J, Kozlov ME, Fang S, Mirfakhrai T, Madden JDW, Shin MK, Kim SJ & Baughman RH (2011) Torsional carbon nanotube artificial muscles. Science 334(6055): 494–497.

Fu Y, Carlberg B, Lindahl N, Lindvall N, Bielecki J, Matic A, Song Y, Hu Z, Lai Z, Ye L, Sun J, Zhang Y, Zhang Y & Liu J (2012) Templated growth of covalently bonded three–dimensional carbon nanotube networks originated from graphene. Advanced Materials 24(12): 1576–1581.

Fujisawa K, Komiyama K, Muramatsu H, Shimamoto D, Tojo T, Kim YA, Hayashi T, Endo M, Oshida K, Terrones M & Dresselhaus MS (2011) Chirality–dependent transport in double–walled carbon nanotube assemblies: the role of inner tubes. ACS Nano 5(9): 7547–7554.

Garcia–Esparza AT, Cha D, Ou Y, Kubota J, Domen K & Takanabe K (2013) Tungsten carbide nanoparticles as efficient cocatalysts for photocatalytic overall water splitting. Chemistry & Sustainability Energy & Materials 6(1): 168–181.

Ghosh A & Lee YH (2012) Carbon–based electrochemical capacitors. Chemistry & Sustainability Energy & Materials 5(3): 480–499.
Gong K, Du F, Xia Z, Durstock M & Dai L (2009) Nitrogen–doped carbon nanotube arrays with high electrocatalytic activity for oxygen reduction. Science 323(5915): 760–764.
Gosselink RW, Stellwagen DR & Bitter JH (2013) Tungsten–based catalysts for selective deoxygenation. Angewandte Chemie International Edition 52(19): 5089–5092.
Gracia E, Sala G, Pino F, Halonen N, Luomahaara J, Mäklin J, Tóth G, Kordás K, Jantunen H, Terrones M, Helistö P, Seppä H, Ajayan PM & Vajtai R (2010) Electrical transport and field effect transistors using inkjet printed SWCNTs films having different functional side groups. ACS Nano 4(6): 3318–3324.
Greeley J, Jaramillo TF, Bonde J, Chorkendorff I & Nørskov JK (2006) Computational high–throughput screening of electrocatalytic materials for hydrogen evolution. Nature Materials 5(11): 909–913.
Grieshaber D, MacKenzie R, Vörös J & Reimhult E (2008) Electrochemical biosensors – sensor principles and architectures. Sensors 8(3): 1400–1458.
Gu Z & Deng B (2007) Use of iron–containing mesoporous carbon (IMC) for arsenic removal from drinking water. Environmental Engineering Science 24(1): 113–121.
Gulotty R, Castellino M, Jagdale P, Tagliaferro A & Balandin AA (2013) Effects of functionalization on thermal properties of single–wall and multi–wall carbon nanotube–polymer nanocomposites. ACS Nano 7(6): 5114–5121.
Guo SJ, Wen D, Zhai YM, Dong SJ & Wang EK (2010) Platinum nanoparticle ensemble–on–graphene hybrid nanosheet: one–pot, rapid synthesis, and used as new electrode material for electrochemical sensing. ACS Nano 4(7): 3959–3968.
Guo W, Liu C, Zhao F, Sun X, Yang Z, Chen T, Chen X, Qiu L, Hu X & Peng H (2013) A novel electromechanical actuation mechanism of a carbon nanotube fiber. Advanced Materials 24(39): 5379–5384.
Halonen N, Kordas K, Toth G, Mustonen T, Maklin J, Vahakangas J, Ajayan PM & Vajtai R (2008) Controlled CCVD synthesis of robust multiwalled carbon nanotube films. The Journal of Physical Chemistry C 112(17): 6723–6728.
Halonen N, Mäklin J, Rautio A–R, Kukkola J, Uusimäki A, Toth G, Reddy LM, Vajtai R, Ajayan PM & Kordas K (2013) Thin micropatterned multi–walled carbon nanotube films for electrodes. Chemical Physics Letters 583: 87–91.
Halonen N, Rautio AAR, Kyllönen T, Tóth G, Lappalainen J, Kordás K, Huuhtanen M, Keiski RL, Sápi A, Szabó M, Kukovecz Á, Kónya Z, Kiricsi I, Vajtai R & Ajayan PM (2010) Three dimensional carbon nanotube scaffolds as filters or catalyst support membranes. ACS Nano 4(4): 2003–2008.
Han SJ, Sohn K & Hyeon T (2000) Fabrication of new nanoporous carbons through silica templates and their application to the adsorption of bulky dyes. Chemistry of Materials 12(11): 3337–3341.
Hartmann M, Vinu A & Chandrasekar G (2005) Adsorption of vitamin E on mesoporous carbon molecular sieves. Chemistry of Materials 17(4): 829–833.

Hata K, Futaba DN, Mizuno K, Namai T, Yumura M & Iijima S (2004) Water–assisted highly efficient synthesis of impurity–free single–walled carbon nanotubes. Science, 306(5700): 1362–1364.

He Y, Chen W, Gao C, Zhou J, Li X & Xie E (2013) An overview of carbon materials for flexible electrochemical capacitors. Nanoscale 5(19): 8799–8820.

Heli H, Jafarian M, Mahjani MG & Gobal F (2004) Electro–oxidation of methanol on copper in alkaline solution. Electrochimica Acta 49(27): 4999–5006.

Helmholtz HV (1853) Ueber einige Gesetze der Vertheilung elektrischer Ströme in körperlichen Leitern, mit Anwendung auf die thierisch–elektrischen Versuche (Schluss.) Annalen der Physik (Leipzig), 89(2): 211–233.

Hinnemann B, Moses PG, Bonde J, Jørgensen KP, Nielsen JH, Horch S, Chorkendorff I & Nørskov JK (2005) Biomimetic hydrogen evolution: MoS_2 nanoparticles as catalyst for hydrogen evolution. Journal of the American Chemical Society 127(15): 5308–5309.

Hiraoka T, Izadi–Najafabadi A, Yamada T, Futaba DN, Yasuda S, Tanaike O, Hatori H, Yumura M, Iijima S & Hata K (2010) Compact and light supercapacitor electrodes from a surface–only solid by opened carbon nanotubes with 2200 m2g–1 surface area. Advanced Functional Materials 20(3): 422–428.

Hou Y, Cheng Y, Hobson T & Liu J (2010) Design and synthesis of hierarchical MnO2 nanospheres/carbon nanotubes/conducting polymer ternary composite for high performance electrochemical electrodes. Nano Letters 10(7): 2727–2733.

Hu G, Nitze F, Sharifi T, Barzegar HR & Wågberg T (2012) Self–assembled palladium nanocrystals on helical carbon nanofibers as enhanced electrocatalysts for electro–oxidation for small molecules. Journal of Materials Chemistry 22(17): 8541–8548.

Hu GZ, Nitze F, Jia X, Gracia–Espino E, Ma JY, Barzegar HR, Sharifi T, Jia XE, Shchukarev A, Lu L, Ma CS, Yang G & Wågberg T (2014) Small palladium islands embedded in palladium–tungsten bimetallic nanoparticles form catalytic hot–spots for oxygen reduction. Nature Communications 5: 5253.

Hu H, Zhao Z, Wan W, Gogotsi Y & Qiu J (2013) Ultralight and highly compressible graphene aerogels. Advanced Materials 25(15): 2219–2223.

Huang J, Sumpter BG & Meunier V (2009) A Universal Model for Nanoporous Carbon Supercapacitors Applicable to Diverse Pore Regimes, Carbon Materials, and Electrolytes. Chemistry – A European Journal 14(22): 6614–6626.

Huber B, Koskinen P, Häkkinen H & Moseler M (2006) Oxidation of magnesia–supported Pd–clusters leads to the ultimate limit of epitaxy with a catalytic function. Nature Materials 5(1): 44 – 47.

Hurt ST, Nimmanwudipong T & Roman–Leshkov Y (2014) Engineering non–sintered, metal–terminated tungsten carbide nanoparticles for catalysis. Angewandte Chemie International Edition 53(20): 5131–5136.

Ibrahim I, Bachmatiuk A, Warner JH, Büchner B, Cuniberti G & Rümmeli MH (2012) CVD–grown horizontally aligned single–walled carbon nanotubes: synthesis routes and growth mechanisms. Small 8(13) 1973–1992.

Iijima S (1991) Helical microtubules of graphitic carbon. Nature 354(6348): 56–58.

Ji N, Zhang T, Zheng M, Wang A, Wang H, Wang X & Chen JG (2008) Direct catalytic conversion of cellulose into ethylene glycol ssing nickel–promoted tungsten carbide catalyst. Angewandte Chemie International Edition 47(44): 8510–8513.

Joo SH, Choi SJ, Oh I, Kwak J, Lin Z, Terasaki O & Ryoo R (2001) Ordered nanoporous arrays of carbon supporting high dispersions of platinum nanoparticles. Nature 412(6843): 169–172.

Kelly BT (1981) Physics of Graphite, Applied Science, London.

Kim KS, Zhao Y, Jang H, Lee SY, Kim JM, Kim KS, Ahn JH, Kim P, Choi JY & Hong BH (2009) Large–scale pattern growth of graphene films for stretchable transparent electrodes. Nature 457(7230): 706–710.

Kis A, Csányi G, Salvetat J–P, Lee T–N, Couteau E, Kulik AJ, Benoit W, Brugger J & Forró L (2004) Reinforcement of single–walled carbon nanotube bundles by intertube bridging. Nature Materials 3(3) 153–157.

Kordás K, Mustonen T, Tóth G, Jantunen H, Lajunen M, Soldano C, Vajtai R & Ajayan PM (2006) Ink–jet printing of electrically conductive patterns of carbon nanotubes. Small 2(8–9): 1021–1025.

Kroto HW, Heath JR, O'Brien SC, Curl RF & Smalley RE (1985) C60: Buckminsterfullerene. Nature 318 (6042): 162–163.

Kyotani T, Yamada H, Sonobe N & Tomita A (1994) Heat treatment of polyfurfuryl alcohol prepared between taeniolite lamellae. Carbon 32(4): 627–635.

Lai CZ, Fierke MA, Stein A & Bűhlmann P (2007) Ion–selective electrodes with three–dimensionally ordered macroporous carbon as the solid contact. Analytical Chemistry 79 (12): 4621–4626.

Lai YY, Cheng YJ & Hsu CS (2014) Applications of functional fullerene materials in polymer solar cells. Energy & Environmental Science 6: 1866–1883.

Lee J, Yoon S, Hyeon T, Oh SM & Kim KB (1999) Synthesis of a new mesoporous carbon and its application to electrochemical double–layer capacitors. Chemical Communications 21: 2177–2178.

Lee J, Yoon S, Hyeon T, Oh SM & Kim KB (1999) Synthesis of a new mesoporous carbon and its application to electrochemical double–layer capacitors. Chemical Communications 21: 2177–2178.

Lee J, Yoon S, Hyeon T, Oh SM & Kim KB (1999) Synthesis of a new mesoporous carbon and its application to electrochemical double–layer capacitors. Chemical Communications 21: 2177–2178.

Lee SW, Kim BS, Chen S, Yang SH & Hammond PT (2009) Layer–by–layer assembly of all carbon nanotube ultrathin films for electrochemical applications. Journal of the American Chemical Society 131(2): 671–679.

Leino Anne–Riikka, Mohl M, Kukkola J, Maki–Arvela P, Kokkonen T, Shchukarev A & Kordas K (2013) Low–temperature catalytic oxidation of multi–walled carbon nanotubes. Carbon 57: 99–107.

Levy RB & Boudart M (1973) Platinum–Like Behavior of Tungsten Carbide in Surface Catalysis. Science 181(4099): 547–549.

Li D, Muller MB, Gilje S, Kaner RB & Wallace GG (2008) Processable aqueous dispersions of graphene nanosheets, Nature Nanotechnology 3(1): 101–105.

Li H, Tee BC–K, Cha JJ, Cui Y, Chung JW, Lee SY & Bao Z (2012) High–mobility field–effect transistors from large–area solution–grown aligned C60 Single Crystals. Journal of the American Chemical Society 134 (5): 2760–2765.

Li JT, Lei W, Zhang XB, Zhou XD, Wang QL, Zhang YN & Wang BP (2003) Field emission characteristic of screen–printed carbon nanotube cathode. Applied Surface Science 220(1–4): 96–104.

Li Q, Fan S, Han W, Sun C & Liang W (1997) Coating of carbon nanotube with nickel by electroless plating method, Japanese Journal of Applied Physics 36 (4B): L501–L503.

Li W, Liang C, Zhou W, Qiu J, Zhou Z, Sun G & Xin Q (2003) Preparation and characterization of multiwalled carbon nanotube–supported platinum for cathode catalysts of direct methanol fuel cells. The Journal of Physical Chemistry B 107(26): 6292–6299.

Liang C & Dai S (2006) Synthesis of mesoporous carbon materials via enhanced hydrogen–bonding interaction. Journal of the American Chemical Society 128(16): 5316–5317.

Liang C, Hong K, Guiochon GA, Mays JW & Dai S (2004) Synthesis of a large–scale highly ordered porous carbon film by self–assembly of block copolymers. Angewandte Chemie International Edition 43(43): 5785–5789

Lin JF, Tu GY, Ho CC, Chang CY, Yen WC, Hsu SH, Chen YF, Su WF (2013) Molecular structure effect of pyridine–based surface ligand on the performance of P3HT:TiO_2 hybrid solar cell. ACS Applied Materials & interfaces 5(3): 1009–1016.

Liu CH & Zhang HL (2010) Chemical approaches towards single–species single–walled carbon nanotubes. Nanoscale 2(10): 1901–1918.

Liu K, Wang W, Xu Z, Bai X, Wang E, Yao Y, Zhang J & Liu Z (2009) Chirality–dependent transport properties of double–walled nanotubes measured in situ on their field–effect transistors. Journal of the American Chemical Society, 131(1): 62–63.

Loh OY & Espinosa HD (2012) Nanoelectromechanical contact switches, Nature Nanotechnology 7(5): 283–295.

Lukowski MA, Daniel AS, English CR, Meng F, Forticaux A, Hamers RJ & Jin S (2014) Highly active hydrogen evolution catalysis from metallic WS_2 nanosheets. Energy & Environmental Science 7(8): 2608–2613.

Luong JHT, Hrapovic S & Wang DS (2005) Multiwall carbon nanotube (MWCNT) based electrochemical biosensors for mediatorless eetection of putrescine. Electroanalysis 17(1): 47–53.

McNicol BD, Rand DAJ & Williams KR (1999) Direct methanol–air fuel cells for road transportation. Journal of Power Sources 83(1–2): 15–31.

Meng G, Jung YJ, Cao A, Vajtai R & Ajayan PM (2005) Controlled fabrication of hierarchically branched nanopores, nanotubes, and nanowires. Proceedings of the National Academy of Sciences of the United States of America 102(20): 7074–7078.

Mertz E, Beil JB & Zimmerman SC (2003) Kinetics and thermodynamics of amine and diamine signaling by a trifluoroacetyl azobenzene reporter group. Organic Letters 5(17): 3127-3130.

Mohl M, Dobo D, Kukovecz A, Konya Z, Kordas K, Wei J, Vajtai R & Ajayan PM (2011) Formation of CuPd and CuPt bimetallic nanotubes by galvanic replacement reaction. The Journal of Physical Chemistry C 115(19): 9403–9409.

Mohr GJ (2004) Chromo– and fluororeactands: indicators for detection of neutral analytes by using reversible covalent–bond chemistry. Chemistry – A European Journal 10(5): 1082–1090.

Moniruzzaman M & Winey, KI (2006) Polymer nanocomposites containing carbon nanotubes. Macromolecules 39(16): 5194–5205.

Morales–Guio CG, Stern L–A & Hu X (2014) Nanostructured hydrotreating catalysts for electrochemical hydrogen evolution. Chemical Society Reviews 43(18): 6555–6569.

Morozov SV, Novoselov KS, Katsnelson MI, Schedin F, Elias DC, Jaszczak JA & Geim AK (2008) Giant intrinsic carrier mobilities in graphene and its bilayer. Physical Review Letters, 100(1): 016602.

Mustonen T, Mäklin J, Kordás K, Halonen N, Tóth G, Vähäkangas J, Jantunen H, Kar S, Ajayan PM, Vajtai R, Helistö P & Seppä H (2008) Controlled ohmic and nonlinear electrical transport in inkjet printed single–wall carbon nanotube films, Physical Review B 77(12): 125430.

Naraghi M, Bratzel GH, Filleter T, An Z, Wei X, Nguyen ST, Buehler MJ & Espinosa HD (2013) Atomistic investigation of load transfer between DWNT bundles "crosslinked" by PMMA oligomers. Advanced Functional Materials 23 (15): 1883–1892.

Naraghi M, Filleter T, Moravsky A, Locascio M, Loutfy RO & Espinosa HD (2010) A multiscale study of high performance double–walled nanotube–polymer fibers. ACS Nano 4 (11): 6463–6476.

Nasibulin AG, Pikhitsa PV, Jiang H, Brown DP, Krasheninnikov AV, Anisimov AS, Queipo P, Moisala A, Gonzalez D, Lientschnig G, Hassanien A, Shandakov SD, Lolli G, Resasco DE, Choi M, Tomanek D & Kauppinen EI (2007) A novel hybrid carbon material. Nature Nanotechnology 2(3): 156–161

Nguyen DD, Tai NH, Leea SB & Kuob WS (2012) Superhydrophobic and superoleophilic properties of graphene–based sponges fabricated using a facile dip coating method. Energy & Environmental Science 5(7): 7908–7912.

Nitze F, Sandström R, Barzegar HR, Hu GZ, Mazurkiewicz M, Malolepszy A, Stobinski L & Wågberg T (2014) Direct support mixture painting, using Pd(0) organo–metallic compounds – an easy and environmentally sound approach to combine decoration and electrode preparation for fuel cells. Journal of Materials Chemistry A 2(48): 20973–20979.

Novoselov KS, Geim AK, Morozov SV, Jiang D, Zhang Y, Dubonos SV, Grigorieva IV & Firsov AA (2004) Electric field effect in atomically thin carbon films. Science 306 (5696): 666–669.

O'Connell MJ, Boul P, Ericson LM, Huffman C, Wang Y, Haroz E, Kuper C, Tour J, Ausman KD, & Smalley RE (2001) Reversible water–solubilization of single–walled carbon nanotubes by polymer wrapping. Chemical Physics Letters 342(3): 265–271.

Peng B, Locascio M, Zapol P, Li S, Mielke SL, Schatz GC & Espinosa HD (2008) Measurements of near–ultimate strength for multiwalled carbon nanotubes and irradiation–induced crosslinking improvements. Nature Nanotechnology 3(10): 626–631.

Pham–Huu C, Keller N, Roddatis VV, Mestl G, Schlögl R & Ledouxa MJ (2002) Large scale synthesis of carbon nanofibers by catalytic decomposition of ethane on nickel nanoclusters decorating carbon nanotubes. Physical Chemistry Chemical Physics 4(3): 514–521.

Pinilla JL, Lázaro MJ, Suelves I & Moliner R (2011) Formation of hydrogen and filamentous carbon over a Ni–Cu–Al2O3 catalyst through ethane decomposition, Applied Catalysis A: General 394(1–2): 220–227.

Pinilla JL, Utrilla R, Lázaro MJ, Moliner R, Suelves I & García AB(2011) Ni– and Fe–based catalysts for hydrogen and carbon nanofilament production by catalytic decomposition of methane in a rotary bed reactor. Fuel Processing Technology 92(8): 1480–1488.

Poncharal P, Wang ZL, Ugarte D & de Heer WA (1999) Electrostatic deflections and electromechanical resonances of carbon nanotubes. Science 283(5407): 1513–1516.

Ratha S & Rout CS (2013) Supercapacitor electrodes based on layered tungsten disulfide–reduced graphene oxide hybrids synthesized by a facile hydrothermal method. ACS Applied Materials & Interfaces 5(21): 11427–11433

Rautio A–R, Pitkänen O, Järvinen T, Samikannu A, Halonen N, Mohl M, Mikkola J–P & Kordas K (2015) Electric double–layer capacitors based on multiwalled carbon nanotubes: can nanostructuring of the nanotubes enhance performance? The Journal of Physical Chemistry C 119(7): 3538–3544.

Raymundo–Pinero E, Kierzek K, Machnikowski J & Begun F (2006) Relationship between the nanoporous texture of activated carbons and their capacitance properties in different electrolytes. Carbon 44(12): 2498–2507.

Rinzler AG, Hafner JH, Nikolaev P, Lou L, Kim SG, Tomanek D, Nordlander P, Colbert DT & Smalley RE (1995) Unraveling Nanotubes: Field Emission from an Atomic Wire. Science 269(5230): 1550–1553.

Rodriguez NM, Chambers A & Baker RTK (1995) Catalytic Engineering of Carbon Nanostructures. Langmuir, 11(10): 3862–3866.

Rogers JA, Someya T & Huang Y (2010) Materials and mechanics for stretchable electronics. Science 327(5973): 1603–1607.

Ryoo R, Joo SH, Kruk M & Jaroniec M (2001) Ordered mesoporous carbons. Advanced Materials 13(9): 677–681.

Saito R, Fujita M, Dresselhaus G & Dresselhaus MS (1992) Electronic structure of chiral graphene tubules. Applied physics letters 60(18): 2204–2206.

Salvetat JP, Briggs GAD, Bonard JM, Bacsa RR, Kulik AJ, Stöckli T, Burnham NA & Forró L (1999) Elastic and Shear Moduli of Single–Walled Carbon Nanotube Ropes. Physical Review Letters 82(5): 944–947.

Salvetat JP, Kulik AJ, Bonard JM, Andrew G, Briggs D, Stöckli T, Méténier K, Bonnamy S, Béguin F, Burnham NA & Forró L (1999) Elastic modulus of ordered and disordered multiwalled carbon nanotubes. Advanced Materials 11(2): 161–165.

Sazonova V, Yaish Y, Űstűnel H, Roundy D, Arias TA & McEuen PL (2004) A tunable carbon nanotube electromechanical oscillator. Nature 431(7006): 284–287.
Shams EI Din AM & Abd EI Wahab FM (1964) The behaviour of the copper electrode in alkaline solutions upon alternate anodic and cathodic polarization. Electrochimica Acta 9(1):113–121.
Shao YY, Wang J, Wu H, Liu J, Aksay IA & Lin YH (2010) Graphene based electrochemical sensors and biosensors: a review. Electroanalysis 22(10): 1027–1036.
Shih ZY, Wang CW, Xub G & Chang HT (2013) Porous palladium copper nanoparticles for the electrocatalytic oxidation of methanol in direct methanol fuel cells. Journal of Materials Chemistry A 1(15): 4773–4778.
Shulaker MM, Hills G, Patil N, Wei H, Chen HY, Wong HSP & Mitra S. (2013) Carbon nanotube computer. Nature 501(7468): 526–530.
Simon P & Gogotsi Y (2008) Materials for electrochemical capacitors. Nature Materials 7(11): 845–854.
Singla G, Singh K & Pandey OP (2015) Effect of processing variables on WC nanoparticles synthesized by solvothermal route. Particulate Science and Technology 33(1): 47–52.
Sobczynski A, Yildiz A, Bard AJ, Campion A, Fox MA, Mallouk T, Webber SE & White JM (1988) Tungsten disulfide: a novel hydrogen evolution catalyst for water decomposition. The Journal of Physical Chemistry 92(8): 2311–2315.
Sridhar S, Ge L, Tiwary CS, Hart AC, Ozden S, Kalaga K, Lei S, Sridhar SV, Sinha RK, Harsh H, Kordas K, Ajayan PM & Vajtai R (2014) Enhanced field emission properties from CNT arrays synthesized on inconel superalloy. ACS Applied Materials & Interfaces 6(3): 1986–1991.
Sridhar S, Tiwary C, Vinod S, Taha–Tijerina JJ, Sridhar S, Kalaga K, Sirota B, Hart AHC, Ozden S, Sinha RK, Harsh H, Vajtai R, Choi W, Kordás K & Ajayan PM (2014) Field emission with ultralow turn on voltage from metal decorated carbon nanotubes. ACS Nano 8(8): 7763–7770.
Stern O (1924) The theory of the electrolytic double–layer. Zeitschrift fuer Elektrochemie und Angewandte Physikalische Chemie 30: 508–516.
Stoller MD, Park S, Zhu Y, An J & Ruoff RS (2008) Graphene–based ultracapacitors. Nano Letters 8 (10): 3498–3502.
Swamy BEK & Venton BJ (2007) Carbon nanotube–modified microelectrodes for simultaneous detection of dopamine and serotoninin vivo. Analyst 132(9): 876–884.
Takagi SH, Toriumi A, Iwase M & Tango H (1994) On the universality of inversion layer mobility in Si MOSFET's: Part I–effects of substrate impurity concentration. IEEE Transactions on Electron Devices 41(12): 2357–2362.
Talapatra S, Kar S, Pal SK, Vajtai R, Ci L, Victor P, Shaijumon MM, Kaur S, Nalamasu O & Ajayan PM (2006) Direct growth of aligned carbon nanotubes on bulk metals. Nature Nanotechnology 1(2): 112–116.
Tian N, Zhou Z–Y, Sun S–G, Ding Y & Wang ZL (2007) Synthesis of tetrahexahedral platinum nanocrystals with high–index facets and high electro–oxidation activity. Science 316(5825): 732–735.

Treacy MMJ, Ebbesen TW & Gibson JM (1996) Exceptionally high Young's modulus observed for individual carbon nanotubes. Nature 381(6584): 678–680.

Tributsch H & Bennett JC (1977) Electrochemistry and photochemistry of MoS_2 layer crystals. Journal of Electroanalytical Chemistry and Interfacial Electrochemistry 81(1): 97–111.

Vickery JL, Patil AJ & Mann S (2009) Fabrication of graphene–polymer nanocomposites with higher–order three–dimensional architectures. Advanced Materials 21(21): 2180–2184.

Vigolo B, Pénicaud A, Coulon C, Sauder C, Pailler R, Journet C, Bernier P & Poulin P (2000) Macroscopic fiber and ribbons of oriented carbon nanotubes. Science 290(5495): 1331–1334.

Voiry D, Yamaguchi H, Li J, Silva R, Alves DCB, Fujita T, Chen M, Asefa T, Shenoy VB, Eda G & Chhowalla M (2013) Enhanced catalytic activity in strained chemically exfoliated WS_2 nanosheets for hydrogen evolution. Nature Materials 12(9): 850–855.

Walter MG, Warren EL, McKone JR, Boettcher SW, Mi Q, Santori EA & Lewis NS (2010) Solar water splitting cells. Chemical Reviews 110(11): 6446–6473.

Wang H, Casalongue HS, Liang Y & Dai H (2010) $Ni(OH)_2$ nanoplates grown on graphene as advanced electrochemical pseudocapacitor materials. Journal of the American Chemical Society 132(21): 7472–7477.

Wang H, Kong D, Johanes P, Cha JJ, Zheng G, Yan K, Liu N & Cui Y (2013) $MoSe_2$ and WSe_2 nanofilms with vertically aligned molecular layers on curved and rough surfaces. Nano Letters 13(7): 3426–3433.

Wang J (2005) Carbon–nanotube based electrochemical biosensors: a review. Electroanalysis, 17(1): 7–14.

Wang X, Zhi L & Müllen K (2008) Transparent, conductive graphene electrodes for dye–sensitized solar cells. Nano Letter 8 (1): 323–327.

Wei BQ, Vajtai R, Jung Y, Ward J, Zhang R, Ramanath G & Ajayan PM (2002) Organized assembly of carbon nanotubes–cunning refinements help to customize the architecture of nanotube structures. Nature 416(6880): 495–496.

Woan K, Pyrgiotakis G & Sigmund W (2009) Photocatalytic carbon–nanotube–TiO_2 composites. Advanced Materials 21(21): 2233–2239.

Wong EW, Sheehan PE & Lieber CM (1997) Nanobeam mechanics: elasiticuty, strength, and toughness of nanorods and nanotubes. Science 277(5334): 1971–1975.

Wu ZS, Sun Y, Tan YZ, Yang S, Feng X & Miilen K (2013) Three–dimensional graphene–based macro– and mesoporous framworks for high–perrformance electrochemical capacitive energy storage. Journal of the American Chemical Society 134(48): 19532–19535.

Xu C, Wu G, Liu Z, Wu D, Meek TT & Han Q (2004) Preparation of copper nanoparticles on carbon nanotubes by electroless plating method. Materials Research Bulletin 39(10): 1499–1505.

Xu D, Liu ZP, Yang HZ, Liu QS, Zhang J, Fang JY, Zou SZ & Sun K (2009) Solution–based evolution and enhanced methanol oxidation activity of monodisperse platinum–copper nanocubes. Angewandte Chemie International Edition 48(23): 4217–4221

Yang ZX, Xia YD & Mokaya R (2007) Enhanced hydrogen storage capacity of high surface area zeolite–like carbon materials. Journal of the American Chemical Society 129(6): 1673–1679.

Yao Y, Li G, Ciston S, Lueptow RM & Gray KA (2008) photoreactive TiO_2/carbon nanotube composites: Synthesis and reactivity. Environmental Science & Technology 42(13): 4952–4957.

Yu MF, Files BS, Arepalli S & Ruoff RS (2000) Tensile loading of ropes of single wall carbon nanotubes and their mechanical properties. Physical Review Letters 84(24): 5552–5555.

Yu MF, Lourie O, Dyer MJ, Moloni K, Kelly TF & Ruoff RS (2000) Strength and breaking mechanism of multiwalled carbon nanotubes under tensile load. Science 287(5453): 637–640.

Zeng W, Shu L, Li Q, Chen S, Wang F & Tao XM (2014) Fiber–based wearable electronics: a review of materials, fabrication, devices, and applications. Advanced Materials 26(31): 5310–5336.

Zhang LL & Zhao XS (2009) Carbon–based materials as supercapacitor electrodes. Chemical Society Reviews 38(9): 2520–2531.

Zhang M, Fang S, Zakhidov AA, Lee SB, Aliev AE, Williams CD, Atkinson KR & Baughman RH (2005) Strong, transparent, multifunctional, carbon nanotube sheets. Science 2005, 309 (5738): 1215–1219.

Zhang Q, Huang JQ, Zhao MQ, Qian W–Z & Wei F (2011) Carbon nanotube mass production: principles and processes. Chemistry & Sustainability Energy & Materials 4(7): 864 – 889.

Zhang Y, Tang ZR, Fu X & Xu YJ (2011) Engineering the unique 2D mat of graphene to achieve graphene–TiO_2 nanocomposite for photocatalytic selective transformation: what advantage does graphene have over Its forebear carbon nanotube? ACS Nano 5 (9): 7426–7435.

Zhang YG, Chang AL, Cao J, Wang Q, Kim W, Li YM, Morris N, Yenilmez E, Kong J & Dai HJ(2001) Electric–field–directed growth of aligned single–walled carbon nanotubes. Applied Physic Letters 79(19): 3155–3157.

Zhao Y, Wei J, Vajtai R, Ajayan PM & Barrera EV (2011) Iodine doped carbon nanotube cables exceeding specific electrical conductivity of metals. Scientific Reports 1: 83.

Zheng M, Jagota A, Semke ED, Diner BA, Mclean RS, Lustig SR, Richardson RE & Tassi NG (2003) DNA–assisted dispersion and separation of carbon nanotubes. Nature Materials 2(5): 338–342.

Zhou H, Zhu S, Hibino M, Honma I & Ichihara M (2003) Lithium storage in ordered mesoporous carbon (CMK–3) with high reversible specific energy capacity and good cycling performance. Advanced Materials 15(24): 2107–2111.

Original papers

I Lin JF, Mohl M, Nelo M, Toth G, Kukovecz Á, Kónya Z, Sridhar S, Vajtai R, Ajayan PM, Su WF, Jantunen H & Kordas K (2015) Facile synthesis of nanostructured carbon materials over Raney® nickel catalyst films printed on Al_2O_3 and SiO_2 substrates. Journal of Materials Chemistry C 3(8): 1823–1829.

II Lin JF, Kukkola J, Sipola T, Raut D, Samikannu A, Mikkola, JP, Mohl M, Toth G, Su WF, Laurila T & Kordas K (2015) Trifluoroacetylazobenzene for optical and electrochemical detection of amines. Journal of Materials Chemistry A 3(8): 4687–4694.

III Lin JF, Mohl M, Toth G, Puskás R, Kukovecz Á & Kordas K (2015) Electrocatalytic properties of carbon nanotubes decorated with copper and bimetallic CuPd nanoparticles. Topics in Catalysis. Manuscript.

IV Lin JF, Pitkänen O, Mäklin J, Puskas R, Kukovecz A, Dombovari A, Toth G & Kordas K (2015) Synthesis of tungsten carbide and tungsten disulfide on vertically aligned multi–walled carbon nanotube forests and its application as non–Pt electrocatalyst for the hydrogen evolution reaction. Journal of Materials Chemistry A. In press.

The original publications are not included in the electronic version of the dissertation.

Book orders:
Granum: Virtual book store
http://granum.uta.fi/granum/

UNIVERSITY OF OULU P.O. Box 8000 FI-90014 UNIVERSITY OF OULU FINLAND

ACTA UNIVERSITATIS OULUENSIS

UNIVERSITY of OULU
OULUN YLIOPISTO

ISBN 978-952-62-0844-2 (Paperback)
ISBN 978-952-62-0845-9 (PDF)
ISSN 0355-3213 (Print)
ISSN 1796-2226 (Online)